Charge Transport in a Graphene Flake Realization of the Sachdev-Ye-Kitaev Model

by

Oguzhan Can

B.Sc., The University of Toronto, 2016

A THESIS SUBMITTED IN PARTIAL FULFILLMENT OF
THE REQUIREMENTS FOR THE DEGREE OF

MASTER OF SCIENCE

in

The Faculty of Graduate and Postdoctoral Studies

(Physics)

THE UNIVERSITY OF BRITISH COLUMBIA

(Vancouver)

August 2018

The following individuals certify that they have read, and recommend to the Faculty of Graduate and Postdoctoral Studies for acceptance, the thesis entitled:

Charge Transport in a Graphene Flake Realization of the Sachdev-Ye-Kitaev Model

submitted by Oguzhan Can in partial fulfillment of the requirements for

the degree of Master of Science

in Physics

Examining Committee:

Marcel Franz, Physics
Supervisor

Ian Affleck, Physics
Supervisory Committee Member

Supervisory Committee Member

Additional Examiner

Additional Supervisory Committee Members:

Supervisory Committee Member

Supervisory Committee Member

Abstract

We address the transport properties of a mesoscopic realization of the Sachdev-Ye-Kitaev (SYK) model which is an exactly solvable system of interacting spinless fermions connected to the black hole physics through the holographic principle. Starting with a recent proposal for simulating the SYK model in a graphene flake in an external magnetic field and extending it by considering leads attached to it, we model a realistic transport experiment and calculate directly measurable quantities featuring non-Fermi liquid signatures of the SYK physics. We show that the graphene flake realization is robust in the presence of leads and that measuring the tunneling current across the leads one can experimentally observe a non-Fermi liquid - Fermi liquid transition by tuning the external magnetic field threading the flake. After establishing the transport signatures of the SYK model near equilibrium using linear response framework, we then derive a formula to extend our results for tunneling current using Keldysh formalism to explore the effects of finite bias voltage across the leads, going beyond equilibrium.

Lay Summary

Very strong interactions between electrons in a metal are well known to give rise to rich physics yet such materials are in general difficult to analyze theoretically. However, a rare exception has emerged recently. In this work, we consider a new and very popular system called the Sachdev-Ye-Kitaev model which has strong interactions and can be solved exactly. This model is very attractive because it is not only accessible analytically but also has certain properties which are mathematically similar to those of black holes due to its very random, strongly interacting nature. We start with a recently proposed experimental realization of this model and study its electrical conductance in the hopes of understanding implications of very strong interactions between electrons.

Preface

All of the results presented in this thesis have been published on the arXiv e-print archive. [Oguzhan Can, Emilian M. Nica, and Marcel Franz. Charge transport in graphene-based mesoscopic realizations of Sachdev-Ye-Kitaev models, *ArXiv e-prints, arXiv:1808.06584 [cond-mat], Aug 2018*] At the time of writing this thesis, this paper has also been submitted to a peer-reviewed journal.

The universal jump we observe in section 2.1 has been discovered, and the finite temperature weak tunneling regime dependencies of the current presented in section 2.3 have been analytically calculated by my supervisor, Marcel Franz who has also provided the initial idea for this project. I have worked out the details of his preliminary analytical calculation for the zero temperature linear response regime using Keldysh path integral formalism (see appendix) and numerically confirmed and extended these results to finite temperature. My collaborator Emilian Nica has later calculated the finite temperature analytical expression for the linear response current, which is a result we refer to yet do not discuss in this thesis but it can be found in the aforementioned publication.

Keldysh saddle point derivation of the general current expression presented in section 2.4, which is my original contribution, is the main result in this thesis and its details can be found in the appendix. It has also been independently derived by Emilian Nica using diagrammatic techniques.

Analytic results in section 2.5 that provide us with a modified form of the saddle point equations incorporating the effects of the reservoirs on the system are Emilian Nica's work. I have performed the numerical solution to these equations which then showed that the low energy SYK physics on the flake is robust in the presence of explicit coupling to the reservoirs.

Contributions of my collaborators to the analytical results described above, which are critical for presentation and completeness of this work are cited appropriately within the text. I have performed all of the numerical work using Python and these calculations are completed on the high performance computing cluster LISA at the Stewart Blusson Quantum Matter Institute (SBQMI), UBC.

Table of Contents

Appendix

List of Figures

Acknowledgements

I would like to thank Emilian Nica, Chengshu Li, Étienne Lantagne-Hurtubise and Ryan Day for interesting and stimulating discussions. I also thank Ilya Elfimov for his support regarding the computing cluster at the SBQMI which was extremely helpful in this project. Special thanks extend to Marcel Franz, my supervisor, for providing the initial idea and patiently advising me throughout this project. Throughout my program, I was supported by the QuEST initiative at the SBQMI. Finally, I thank my parents Seyhan Can and Abdullah Can for their unconditional support.

For my parents who have always supported me. Most recently, completion of this thesis would not have been possible without the delicious baklavas they made.

Chapter 1

The Model

1.1 Introduction to SYK model and the proposal

SYK is an exactly solvable quantum mechanical model connected to black hole physics in AdS_2 space-time gravity theories through holographic principle. [1] Complex fermion variant of the SYK model is given by

$$H_{\text{SYK}} = \frac{1}{(2N)^{3/2}} \sum_{ijkl} J_{ijkl} c_i^\dagger c_j^\dagger c_k c_l$$

where the couplings among N spinless fermionic modes, J_{ijkl} are drawn from complex random Gaussian distribution with variance $\overline{|J_{ijkl}|^2} = J^2$. This model develops an emergent conformal symmetry [2] at low energies, for $1 \ll \beta J \ll N$. In this so called conformal regime, SYK model displays holographic behaviour such as saturating the chaos bound [3] and finite zero temperature entropy [4] which are also properties of charged black holes. [5]

Though SYK is not the first holographic model, it is remarkable due to its simplicity and the fact that it is exactly solvable. [6] This makes the model crucial in further understanding of the AdS/CFT correspondence which is also called the holographic duality. Holography relates two seemingly unrelated physical systems in the sense that the correlators and certain thermodynamic quantities of the two theories show the same functional dependence [5] and the symmetries of these two theories match [7]

SYK and its variants are popular examples of holographic quantum matter where non-Fermi liquid (NFL) behaviour is observed in the presence of strong correlations and strong disorder. In a non-Fermi liquid, elementary excitations of the system can not be associated with non interacting electronic excitations through adiabatic continuity arguments. This means that the familiar quasiparticle description fails, making theoretical considerations difficult. Nevertheless, SYK model is special: despite the strong correlations it can be solved and certain observable quantities can be analytically obtained [6]. However, the distinct non-Fermi liquid behaviour of SYK model remains to be experimentally observed. Recently, various realizations have

been proposed involving ultracold atoms [8], Majorana modes on the surface of a topological superconductor [9], semiconductor quantum wires attached to a quantum dot [10] and finally a graphene flake in external magnetic field [11], See a recent review [12] for a comprehensive overview of these different approaches. Our focus will be the complex fermion realization of the SYK model utilizing the highly degenerate zeroth Landau levels on a graphene flake in external transverse magnetic field [11]. Though it is shown that such a model realizes the SYK hamiltonian, an actual experimental situation and the quantities that would be measured in a laboratory setup are relatively unexplored.

In this work, we model a transport experiment that would probe the conformal behaviour of the SYK model with this graphene flake realization by attaching two leads that would drive a current through the flake hosting the SYK model. We address the signatures of the conformal SYK behaviour in a transport experiment, effects of attaching the leads to the original model and in particular, study whether the SYK behaviour is robust in the presence of leads. We start with a rather conventional linear response approach near equilibrium and then extend our results to nonequilibrium phenomena.

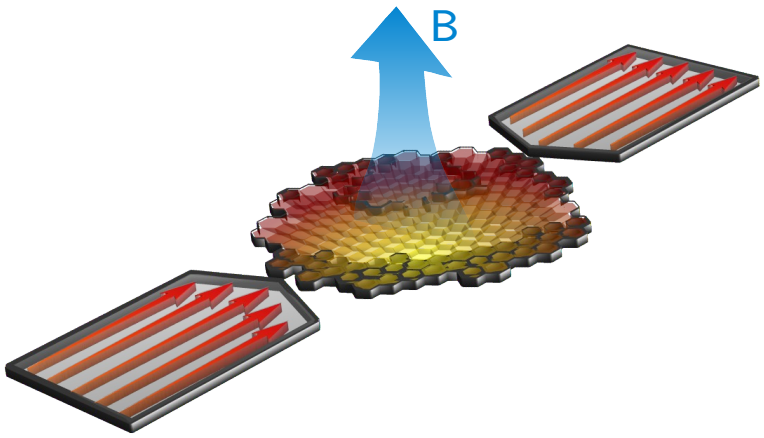

Figure 1.1: A schematic of the proposed experimental setup

In order to study the effects of the leads, we consider an interesting extension of SYK model, proposed by Banerjee and Altman [13], which is an SYK model of N complex fermions coupled to a set of M auxiliary non interacting fermionic degrees of freedom. The authors have shown that by tuning only the fermion density of the SYK model, one observes a quantum phase

transition from a Fermi liquid to a non-Fermi liquid. A remarkable result they obtain is that the phase diagram of this model does not depend on the strength of the coupling between these two sub-systems but only on the SYK fermion density and the ratio of the number of fermions $p = M/N$ constitute the two. Just as in the original SYK model, this system is also exactly solvable in the large-N, M limit. *We propose that the extension of SYK model by Banerjee and Altman [13] can be adapted to the graphene flake realization [11] where the noninteracting auxiliary fermions would model the endpoints of leads coupled to graphene flake which hosts SYK complex fermions.* Once such a system is realized in an experimental setting, through a simple transport experiment that only requires readily available technologies, we could obtain the experimental signatures of the SYK model in the large-N limit where the numerical techniques run into difficulties. This model would not only make it possible to probe holographic matter, but also make the experimental study of the predicted Fermi liquid - non-Fermi liquid transition [13] possible, in the hopes of confirming the theoretical predictions.

We also demonstrate that the random Gaussian model for the lead endpoints is not absolutely necessary and we consider a lead model made of noninteracting ballistic chains attached to the SYK graphene flake and show that the SYK physics persists even in the presence of strong coupling to such leads.

1.2 Roadmap

An outline of this thesis is the following. In chapter 1, we first introduce the Banerjee-Altman model [13] briefly (section 1.3) and generalize it to our experimental setup proposal. In section 1.4 we present the equations of motion we solve in Keldysh formalism. These equations are valid beyond equilibrium and can be reduced to the Banerjee-Altman model equations of motion in equilibrium.

In chapter 2, we study the transport properties of the system. We study the system near equilibrium in two separate regimes we call "linear response regime" (section 2.1) and the "weak tunneling regime" (section 2.3). We then derive an expression (section 2.4) for the current at saddle point which is valid in equilibrium and beyond. We then show that the numerical results obtained with this formula match weak tunneling results near equilibrium (section 2.4.1). Next, we turn to linear response regime and again show that the formula we derived matches the linear response regime results (2.4.2). Finally, we go beyond equilibrium and explore the I-V characteristics for

finite bias voltage across the two leads. Up to this point, we have assumed that the lead endpoints are in equilibrium with reservoirs but have not considered their effect on the spectral densities of the leads for simplicity of the model. We justify this assumption in section 2.5 and reproduce some of the results we had in earlier sections in the presence of explicit coupling to the reservoirs. We find that the SYK signatures we predict in transport observables are robust even when the the graphene flake is strongly coupled to the reservoirs.

1.3 Starting Point - BA model in equilibrium

We start our discussion by reviewing the variant of the SYK model proposed by Banerjee and Altman [13]. The model couples the original N complex fermion SYK_4 model H_c to a set of M auxiliary noninteracting fermionic degrees of freedom H_ψ which are also random disordered (which we will call SYK_2). The couplings $H_{c\psi}$ between these two systems are again random disordered. The model is given by the following Hamiltonian:

$$H_c = \frac{1}{(2N)^{3/2}} \sum_{ijkl} J_{ijkl} c_i^\dagger c_j^\dagger c_k c_l - \mu \sum_i c_i^\dagger c_i \tag{1.1}$$

$$H_\psi = \frac{1}{(M)^{1/2}} \sum_{ij} t_{ij} \psi_i^\dagger \psi_j - \mu \sum_i \psi_i^\dagger \psi_i \tag{1.2}$$

$$H_{c\psi} = \frac{1}{(NM)^{1/4}} \sum_{ij} V_{ij} c_i^\dagger \psi_j + V_{ij}^* \psi_j^\dagger c_i \tag{1.3}$$

where $\{J_{ijkl}\}$, $\{t_{ij}\}$ and $\{V_{ij}\}$ are random Gaussian distributions with variances defined as $\overline{|J_{ijkl}|^2} = J^2$, $\overline{|t_{ij}|^2} = t^2$ and $\overline{|V_{ij}|^2} = V^2$ where antisymmetrization and Hermiticity of H_c implies

$$J_{jikl} = -J_{ijkl} \qquad J_{ijlk} = -J_{ijkl} \qquad J_{klij} = -J_{ijkl}^* \tag{1.4}$$

since H_ψ must also be Hermitian,

$$t_{ji} = t_{ij}^* \tag{1.5}$$

We shall start with this Banerjee-Altman model (which we shall refer to as BA from now on) which has only one set of auxiliary fermions (modeled by H_ψ) and then extend it to two auxiliary flavours of fermions which are modeled as the endpoints of the leads attached to the SYK_4 graphene flake

quantum dot (which will correspond to H_c). In the following we use the terms "graphene flake", "quantum dot" or "the dot" interchangably.

Let us first review their main results that are relevant to our model. BA model displays a quantum phase transition between a non-Fermi liquid (NFL) and a Fermi liquid (FL) which is controlled by only two parameters $p = M/N$, and the total fermion density $n = (N\langle n_c\rangle + M\langle n_\psi\rangle)/(M+N)$. At half filling, $n = 1/2$, the NFL/FL transition occurs are $p = p_c = 1$. Away from half filling, this transition occurs at lower values of $p = p_c < 1$, depending on the value of n. A remarkable feature of this transition is that p_c marking the transition does not depend on any of the parameters t, V or J but n only. They show that in the NFL phase, though in the presence of the coupling to the auxiliary fermions, the model has finite zero temperature entropy and it saturates the chaos bound [3] as expected of the SYK model. However, once the transition occurs, the zero temperature entropy vanishes and the model is not maximally chaotic anymore.

Here we copy the saddle point equations [13] that are obtained in Matsubara imaginary time formalism after disorder averaging the action. We will later derive a similar set of equations in Keldysh formalism since we are also interested in nonequilibrium properties of this model. Going back to the BA model, the saddle point equations in Matsubara frequencies are given by:

$$G^{-1}(i\omega_n) = i\omega_n + \mu - \Sigma_J(i\omega_n) - V^2\sqrt{p}\mathcal{G}(i\omega_n)$$

$$\mathcal{G}^{-1}(i\omega_n) = i\omega_n + \mu - \frac{V^2}{\sqrt{p}}G(i\omega_n) - t^2\mathcal{G}(i\omega_n)$$

where $G(\tau) = -\overline{\langle \hat{T}c(\tau)c^\dagger(0)\rangle}$ and $\mathcal{G}(\tau) = -\overline{\langle \hat{T}\psi(\tau)\psi^\dagger(0)\rangle}$ are the disorder averaged imaginary time ordered Green's functions. The saddle point equations above can be analytically continued to:

$$G_R^{-1}(\omega) = \omega + \mu - \Sigma_J^R(\omega) - V^2\sqrt{p}\mathcal{G}_R(\omega)$$

$$\mathcal{G}_R^{-1}(\omega) = \omega + \mu - \frac{V^2}{\sqrt{p}}G_R(\omega) - t^2\mathcal{G}(\omega)$$

In the conformal limit, analytical solution to above equations can be obtained. For the NFL phase, (at half filling, $n = 1/2$ or $\theta = 0$ where $p < p_c = 1$):

$$G_R(\omega) = \frac{\Lambda e^{-i\pi/4}}{\sqrt{J\omega}} \qquad \mathcal{G}_R(\omega) = -\sqrt{p}\frac{\sqrt{J\omega}e^{i\pi/4}}{V^2\Lambda}$$

$$\Sigma_J^R(\omega) = -\frac{\Lambda^3}{\pi} e^{i\pi/4}\sqrt{J\omega}$$

This holds when $\omega \ll \Sigma_J^R(\omega)$ and $\omega \ll V^2\sqrt{p}\mathcal{G}_R(\omega)$ such that the first equation becomes $G_R^{-1}(\omega) = -\Sigma_J^R(\omega) - V^2\sqrt{p}\mathcal{G}_R(\omega)$ and $t^2\mathcal{G}_R(\omega) \ll V^2/\sqrt{p}G_R(\omega)$ as well as $\omega \ll V^2/\sqrt{p}G_R(\omega)$ such that $\mathcal{G}_R^{-1}(\omega) = -\frac{V^2}{\sqrt{p}}G_R(\omega)$ which can be substituted back into the previous equation. We then obtain the same form as the original SYK model saddle point equations. The above four inequalities define four critical frequencies below which the solutions above are justified [13]:

$$\omega_{c1} = \frac{J}{2\sqrt{\pi}}(1-p)^{3/2} \qquad \omega_{c2} = \frac{J}{2\sqrt{\pi}}\frac{p^2}{\sqrt{1-p}}$$

$$\omega_{c3} = \left(\frac{\sqrt{\pi}V^4}{2J}\frac{\sqrt{1-p}}{p}\right)^{1/3} \qquad \omega_{c4} = \frac{\sqrt{\pi}V^4}{t^2 J}\frac{\sqrt{1-p}}{p} \tag{1.6}$$

The conformal solution then holds when all four inequalities hold [13]

$$\omega \ll \min(\omega_{c1} + \omega_{c2}, \omega_{c3}, \omega_{c4})$$

1.3.1 Extending to two symmetric leads

Generalization to two auxiliary and identical SYK_2 models (with M fermions each) is straightforward. Now we relabel $\mathcal{G}$ auxiliary fermion Green's functions as $\mathcal{G}^{(L)}$ for the left lead and introduce $\mathcal{G}^{(R)}$ for the right lead which couples in the same way as $\mathcal{G}^{(L)}$ since we have two identical leads (note that for the lead Green's functions below the subscript R means the retarded Green's function while the superscript (L/R) is the site index corresponding to left and right leads respectively):

$$G_R^{-1}(\omega) = \omega + \mu - \Sigma_J^R(\omega) - V^2\sqrt{p}\left(\mathcal{G}_R^{(L)}(\omega) + \mathcal{G}_R^{(R)}(\omega)\right)$$

$$(\mathcal{G}_R^{(L)})^{-1}(\omega) = \omega + \mu - \frac{V^2}{\sqrt{p}}G_R(\omega) - t^2\mathcal{G}_R^{(L)}(\omega)$$

$$(\mathcal{G}_R^{(R)})^{-1}(\omega) = \omega + \mu - \frac{V^2}{\sqrt{p}}G_R(\omega) - t^2\mathcal{G}_R^{(R)}(\omega)$$

If we take two symmetric leads, we can then take $\mathcal{G}_R^{(R)}(\omega) = \mathcal{G}_R^{(L)}(\omega) = \mathcal{G}_R(\omega)$. If we also define $\tilde{V} = 2^{1/4}V$ and $\tilde{p} = 2p$, then above equations reduce to

$$G_R^{-1}(\omega) = \omega + \mu - \Sigma_J^R(\omega) - \tilde{V}^2\sqrt{\tilde{p}}\mathcal{G}_R(\omega)$$

$$\mathcal{G}_R^{-1}(\omega) = \omega + \mu - \frac{\tilde{V}^2}{\sqrt{\tilde{p}}} G_R(\omega) - t^2 \mathcal{G}_R(\omega)$$

But these equations have the same form as the original BA model. Therefore, everything we know about the BA model holds except that V and p are renormalized. For instance the FL/NFL transition occurs at $2p = \tilde{p} = 1$. **Therefore we expect to see the FL/NFL transition at $p = 0.5$ in this extended model.** Then the NFL solutions for the identical lead case

$$G_R(\omega) = \frac{\Lambda e^{-i\pi/4}}{\sqrt{J\omega}} \tag{1.7}$$

$$\mathcal{G}_R^{(R)}(\omega) = \mathcal{G}_R^{(L)}(\omega) = -\sqrt{p} \frac{\sqrt{J\omega} e^{i\pi/4}}{V^2 \Lambda} \tag{1.8}$$

(note that we used the ratio $\sqrt{\tilde{p}}/\tilde{V}^2 = \sqrt{p}/V^2$ nevertheless we get the same form for the solution.) In the Fermi liquid case, ($p > p_c = 0.5$), the Green's functions (two symmetrical leads) are found to be

$$G_R(\omega) = -\frac{it}{\sqrt{2}V^2} \frac{1}{\sqrt{2p-1}} \tag{1.9}$$

$$\mathcal{G}_R^{(L)}(\omega) = \mathcal{G}_R^{(R)}(\omega) = \mathcal{G}_R(\omega) = -\frac{i}{t} \sqrt{\frac{2p-1}{2p}} \tag{1.10}$$

In this case, the critical frequencies below which we observe conformal regime become

$$\omega_{c1} = \frac{J}{2\sqrt{\pi}} (1-2p)^{3/2} \tag{1.11}$$

$$\omega_{c2} = \frac{2J}{\sqrt{\pi}} \frac{p^2}{\sqrt{1-2p}} \tag{1.12}$$

$$\omega_{c3} = \left(\frac{\sqrt{\pi} V^4}{J} \frac{\sqrt{1-2p}}{2p} \right)^{1/3} \tag{1.13}$$

$$\omega_{c4} = \frac{\sqrt{\pi} V^4}{t^2 J} \frac{\sqrt{1-2p}}{p} \tag{1.14}$$

note that as we tune p, near $p = 0.5$, $\omega_c = min(\omega_{c1} + \omega_{c2}, \omega_{c3}, \omega_{c4})$ becomes arbitrarily small. Therefore, **at the FL/NFL transition we expect to leave conformal regime** as we tune p through $p_c = 0.5$ at particle hole symmetry. This also implies that outside the conformal regime, the analytical forms (1.7) will start showing corrections even at arbitrarily low energies. We will see consequences of this in the following sections.

1.4 Keldysh Formalism for Beyond Equilibrium

In order to study far from equilibrium transport properties and beyond linear response, we have to resort to more advanced Keldysh formalism. Results we obtain here will be more general and should reduce to equilibrium results that we considered in previous section. Following the same formalism as an earlier study [14], we work with Keldysh time contour path integral as opposed to the imaginary time path integrals in Matsubara formalism. See the appendix for the details of the saddle point approximation (Section A.1) for Keldysh action. The saddle point equations in real time are given by:

$$\Sigma^{c}_{ss'}(t) = ss' J^2 G^2_{ss'}(t) G_{s's}(-t) + ss'\sqrt{p}V^2 \mathcal{G}_{L,ss'}(t) + ss'\sqrt{p}V^2 \mathcal{G}_{R,ss'}(t) \quad (1.15)$$

$$\Sigma^{\psi L}_{ss'}(t) = ss' t^2 \mathcal{G}_{L,ss'}(t) + ss'(1/\sqrt{p})V^2 G_{ss'}(t) \quad (1.16)$$

$$\Sigma^{\psi R}_{ss'}(t) = ss' t^2 \mathcal{G}_{R,ss'}(t) + ss'(1/\sqrt{p})V^2 G_{ss'}(t) \quad (1.17)$$

along with the Dyson's equations in frequency space

$$G_{ss'}(\omega) = [\sigma^z(\omega+\mu) - \Sigma^c]^{-1}_{ss'} \quad (1.18)$$

$$\mathcal{G}_{L,ss'}(\omega) = \left[\sigma^z(\omega+\mu) - \Sigma^{\psi L}\right]^{-1}_{ss'} \quad (1.19)$$

$$\mathcal{G}_{R,ss'}(\omega) = \left[\sigma^z(\omega+\mu) - \Sigma^{\psi R}\right]^{-1}_{ss'} \quad (1.20)$$

where $G, \mathcal{G}_L$ and $\mathcal{G}_R$ are the time contour Green's functions of the dot, left and right leads respectively. They have the matrix form $G_{ss'}$ which is defined as:

$$G = \begin{pmatrix} G^T & G^< \\ G^> & G^{\tilde{T}} \end{pmatrix} = \begin{pmatrix} G_{++} & G_{+-} \\ G_{-+} & G_{--} \end{pmatrix}$$

where G^T and $G^{\tilde{T}}$ are the time ordered and anti-time ordered Green's functions, respectively. $G^<$ and $G^>$ are the lesser and the greater Green's functions. These four quantities are not independent. By construction, they are related by $G^T + G^{\tilde{T}} = G^< + G^>$. Path segment index s (takes values of ± 1 in the equations (1.15-1.17) for forward $(+)$ and backward $(-)$ parts of the contour respectively) is the real time path index which appears since we split the time loop contour into two pieces defined on real time axis. In above form we assumed time translational invariance, ignoring the transient behaviour as the couplings are turned on over the time contour path. The following expression of fluctuation-dissipation theorem allows us

to introduce temperature in equilibrium:

$$G^K(\omega) = 2i \tanh\left(\frac{\beta\omega}{2}\right) \mathrm{Im}G^R(\omega). \tag{1.21}$$

where the Keldysh correlator G^K is defined to be $G^K = G^< + G^>$

We solve these equations (1.15-1.20) iteratively while imposing the condition (1.21) for parts of the system which are in equilibrium with a reservoir.

Chapter 2

Transport Properties of the Quantum Dot

We are interested in evaluating the conductance or current between two leads attached to the dot. Since we will limit ourselves to steady state transport, it is sufficient that we consider transport between one of the leads and the dot. The current should be the same between the dot and the other lead since the total charge must be conserved and there is no charge accumulation on the dot in the steady transport state.

There are two standard regimes we explore near equilibrium. The first one is the case where the bias voltage between two leads is smaller than all the other scales in the system so that we can treat the bias as a perturbation. Then, we define equilibrium as the state where the bias difference between two sites of interest is zero. This condition can also be stated as that the chemical potential is identical among all parts if the system thus the electrons have no tendency to jump from one site to the other on average. We will call this the "*linear response regime*".

The other case we can treat near equilibrium is where we start with a finite, arbitrary bias difference between sites but initially these sites, namely the dot and the lead, are decoupled. We then turn on the perturbation as the coupling between two sites, allowing electrons to tunnel between two systems. As long as the coupling parameter is smaller than all the other scales in system, this approach is justified. Following the convention in the literature, we will call this regime the "*weak-tunneling regime*".

What these two approaches have in common is that we start with an equilibrium state and perturb the system slightly. As long as the perturbation is small, our approach is valid. However, we run into difficulties if we would like to go far from equilibrium. First, linear response approach is called 'linear' because we truncate the S-matrix expansion to first order in perturbation δH in order to obtain the expression (2.1). If the perturbation is large, we would have to take the full S-matrix into account. Second, when we calculate the correlators, standard quantum field theory approach where we start with a noninteracting ground state in the distant past and

turn on and off the interactions adiabatically in the distant past and future respectively is not valid since there is the implicit assumption that after we turn off the interactions the state we end up with is identical (up to a phase factor) to the ground state we started with. This assumption does not hold for a generic time dependent Hamiltonian where the system is not in equilibrium. One way to resolve this issue is that instead of considering the evolution of the system from distant past to distant future, one introduces a "time loop contour" that starts from a ground state in the distant past, evolves the system forward in time to the future and then backwards all the way to ground state we started from in the distant past, defining a closed loop. In this approach, we have only one noninteracting ground state we work with, therefore we do not run into the issue we described above in nonequilibrium situations. An additional problem we run into is specific to disorder averaging which is the crucial step that makes the SYK model solvable. Consider the generic correlator

$$\langle \hat{T}_{\mathcal{C}} c_a^\dagger(\tau_1) d_b(\tau_2) \rangle = \frac{\int_{\mathcal{C}} \mathcal{D}[c,d] \overline{c_a}(\tau_1) d_b(\tau_2) e^{iS}}{\int_{\mathcal{C}} \mathcal{D}[c,d] e^{iS}}$$

Regardless of the formalism we use, Keldysh or Matsubara, expressions are structurally the same. If the action S, however, contains random Gaussian variables that need disorder averaging, note that the same variable would appear in both the numerator and denominator. It is not immediately clear how to proceed with disorder averaging due to the path integral in the denominator since the disorder averaging must be carried out simultaneously for both the numerator and the denominator before evaluating the path integrals to obtain an effective action. In Matsubara formalism, this issue can be avoided by introducing the 'replica trick' (as illustrated in [13, 15]) In contrast, in Keldysh formalism, the denominator is identically unity, therefore it does not need to be evaluated. [16] Thus, it suffices to disorder average only the numerator while completely omitting the denominator. The price we pay for this convenience is that we have to promote the saddle point equations and the Dyson's equations to matrix equations which we have to resort to regardless since we are interested in nonequilibrium physics. Therefore, Keldysh formalism will be the ideal tool to study the nonequilibrium transport properties of the SYK model.

In the following, our approach will be to study the two aforementioned limits near equilibrium, and then try to bridge the two in nonequilibrium territory by deriving a more general formula using Keldysh formalism.

2.1 Linear Response

Linear response formalism allows us to extract transport quantities provided that we do not perturb the system far from equilibrium. For a generic expectation value $\langle A(t)\rangle$ of an observable operator A, we need to evaluate the following expression:

$$\langle A(t)\rangle = \langle A\rangle_0 - i\int_{-\infty}^{t} \langle [A(t), \delta H(t')]\rangle_{H_0} dt' \tag{2.1}$$

where the Hamiltonian $H = H_0 + \delta H$ consists of the Hamiltonian H_0 of the system in the absence of perturbation that leads to response and the perturbation δH, typically coupling to an external system or a gauge field which leads to response. The correlators one needs to calculate in linear response formalism are defined with respect to the equilibrium state ($\delta H = 0$), where Matsubara formalism can be used at finite temperature.

Introducing the minimal coupling in the linear response regime

We start with a generic Hamiltonian H made of c and ψ operators living on the quantum dot and the lead respectively. We define the Hamiltonians H_c for the dot and H_ψ the lead. Assuming $[H_c, H_\psi] = 0$, we further introduce the coupling $H_{c\psi}$ between these two systems. Then we can write the Hamiltonian for the coupled system:

$$H = H_c + H_\psi + H_{c\psi}$$

where

$$H_{c\psi} = \sum_{ij} V_{ij} c_i^\dagger \psi_j + V_{ij}^* \psi_j^\dagger c_i$$

We are interested in the linear response regime where the coupling above is fully taken into account to all orders. We introduce a small chemical potential difference between two sites and treat this difference as the perturbation in the linear response regime. This can be achieved by introducing the minimal coupling in H_{cd}

$$V_{ij} \Longrightarrow V_{ij} e^{-i\frac{e}{c}\int_i^j \vec{A}.\vec{dl}}$$

here the gauge field $\vec{A}$ will be related to the potential difference U between two sites. In linear response approximation, we expand the perturbed Hamiltonian to first order in $\vec{A}$, and write the perturbation δH due to minimal

coupling separately:

$$\delta H = -i\frac{e}{c}\int \vec{A}.\vec{dl}\left(\sum_{ij} V_{ij}c_i^\dagger\psi_j - V_{ij}^*\psi_j^\dagger c_i\right)$$

Here we take $\vec{A} = \frac{ic}{\omega}\vec{E}_0 e^{i\omega t}$ since it must hold that $\vec{E} = -\frac{1}{c}\frac{\partial\vec{A}}{\partial t}$ and assume that $\vec{E}_0$ is constant throughout the intermediate region between two sites. We label the length of this region by $\vec{a}$. Then, the above expression can be rewritten in terms of the potential difference between the lead and the dot $U/2 = \vec{E}.\vec{a}$ as

$$\delta H(t) = \frac{eUe^{i\omega t}}{2\omega}\sum_{ij} V_{ij}c_i^\dagger\psi_j - V_{ij}^*\psi_j^\dagger c_i$$

recall that the current operator can be written as

$$I = -ie\sum_{ij} V_{ij}c_i^\dagger\psi_j - V_{ij}^*\psi_j^\dagger c_i \tag{2.2}$$

therefore we obtain:

$$\delta\hat{H}(t) = \frac{i}{\omega}\frac{U}{2}e^{i\omega t}\hat{I}(t)$$

Then we use the linear response expression (2.1) for δH and assuming $\langle I\rangle_0 = 0$ since we do not expect a current in the absence of external field:

$$\langle I(t)\rangle = \frac{U}{2\omega}\int_{-\infty}^{t}\langle[\hat{I}(t),\hat{I}(t')]\rangle_{\delta H=0}e^{i\omega t'}dt' \tag{2.3}$$

$$= i\frac{U}{2\omega}\int_{-\infty}^{\infty}\underbrace{-i\theta(t-t')\langle[\hat{I}(t),\hat{I}(t')]\rangle_{\delta H=0}}_{C_{II}^R(t-t')}e^{i\omega t'}dt' \tag{2.4}$$

where we defined $C_{II}^R(t-t') = -i\theta(t-t')\langle[I(t),I(t')]\rangle_{\delta H=0}$ is the retarded current current correlator between the lead and the dot.

$$\langle I(t)\rangle = \frac{iU}{2\omega}\int_{-\infty}^{\infty}C_{II}^R(t-t')e^{i\omega t'}dt' \tag{2.5}$$

$$= -\frac{iU}{2\omega}e^{i\omega t}\underbrace{\int_{-\infty}^{\infty}C_{II}^R(t-t')e^{-i\omega(t-t')}d(t-t')}_{C_{II}^R(\omega)} \tag{2.6}$$

Where we multiplied and divided the expression by $e^{i\omega t}$ and then changed the integration variable $dt' \to d(t-t')$ Therefore we arrive at an expression for the current between two sites given the potential difference U between is given:

$$\langle I(t)\rangle = \underbrace{-\frac{i}{2\omega}C^R_{II}(\omega)}_{\sigma(\omega)} U e^{i\omega t}$$

The observed quantity would be the conductance:

$$\boxed{\mathrm{Re}[\sigma(\omega)] = \frac{\mathrm{Im}C^R_{II}(\omega)}{2\omega}}$$

This current current correlator can be obtained using Keldysh time contour formalism. We need to evaluate the time contour correlator

$$C_{II}(\tau_1,\tau_2) = -i\langle \hat{T}_C I(\tau_1) I(\tau_2)\rangle$$

at saddle point, this expression is found to be (see appendix A.2 for details)

$$C_{II}(\tau_1,\tau_2) = -ie^2V^2\sqrt{NM}\left[G(\tau_1,\tau_2)\mathcal{G}(\tau_2,\tau_1) + \mathcal{G}(\tau_1,\tau_2)G(\tau_2,\tau_1)\right] \quad (2.7)$$

where G is the time contour Green's function for c operators living on the dot while $\mathcal{G}$ represents the Green's function for the lead operators d Here τ_1, τ_2 are defined on the Keldysh contour. We can analytically continue this expression to obtain $\mathrm{Im}C^R_{II}(t_1,t_2)$. The retarded correlator C^R_{II} in real time is defined as:

$$C^R_{II}(t_1,t_2) = -i\theta(t_1-t_2)\langle[I(t_1),I(t_2)]\rangle \quad (2.8)$$

$$= -i\theta(t_1-t_2)(\underbrace{\langle I(t_1)I(t_2)\rangle}_{iC^<_{II}(t_1^+,t_2^-)} - \underbrace{\langle I(t_2)I(t_1)\rangle}_{iC^>_{II}(t_1^-,t_2^+)}) \quad (2.9)$$

note that $C^<_{II}$ and $C^>_{II}$ can be obtained by anaylytically continuing time contour correlator (2.7) refer to appendix A.3.3. We then obtain

$$C^<_{II}(t_1^+,t_2^-) = -ie^2V^2\sqrt{NM}\left[G^<(t_1,t_2)\mathcal{G}^>(t_2,t_1) + (G\leftrightarrow\mathcal{G})\right]$$
$$C^>_{II}(t_1^-,t_2^+) = -ie^2V^2\sqrt{NM}\left[G^>(t_1,t_2)\mathcal{G}^<(t_2,t_1) + (G\leftrightarrow\mathcal{G})\right]$$

if we plug in these expressions into (2.8) and assuming time translational invariance (ignoring transient response) we get

$$C^R_{II}(t) = -ie^2V^2\sqrt{NM}\theta(t)[G^<(t)\mathcal{G}^>(-t) + \mathcal{G}^<(t)G^>(-t) - G^>(t)\mathcal{G}^<(-t) - \mathcal{G}^>(t)G^<(-t)] \quad (2.10)$$

Fourier transforming,

$$C^R_{II}(\omega) = e^2V^2\sqrt{NM}\int \frac{d\omega_1}{2\pi}\frac{d\omega_2}{2\pi}\frac{G^<(\omega_1)\mathcal{G}^>(\omega_2) - G^>(\omega_1)\mathcal{G}^<(\omega_2)}{\omega_1-\omega_2-\omega+i\delta}+(G\leftrightarrow\mathcal{G})$$

since we are dealing with equilibrium Green's functions we also have $G^<(\omega) = in_F(\omega)A(\omega)$ and $G^>(\omega) = -i(1-n_F(\omega))A(\omega)$ and likewise for $\mathcal{G}$ Green's functions. Taking the imaginary part,

$$\mathrm{Im}C^R_{II}(\omega) = -\frac{\pi e^2V^2\sqrt{NM}}{2\pi}\int\frac{d\omega_1}{2\pi}G^<(\omega_1)\mathcal{G}^>(\omega_1-\omega)-G^>(\omega_1)\mathcal{G}^<(\omega_1-\omega) + (G\leftrightarrow\mathcal{G}) \quad (2.11)$$

using the relation between lesser and greater Green's functions and the spectral functions in equilibrium, we arrive at:

$$\mathrm{Im}C^R_{II}(\omega) = \frac{\pi e^2V^2\sqrt{NM}}{4\pi^2}\int d\omega_1[n_F(\omega_1-\omega)-n_F(\omega_1)][A(\omega_1)\mathcal{A}(\omega_1-\omega)+ \mathcal{A}(\omega_1)A(\omega_1-\omega)] \quad (2.12)$$

$$\langle I(t)\rangle = \underbrace{\frac{\mathrm{Im}C^R_{II}(\omega)}{2\omega}}_{\sigma(\omega)}U = \frac{1}{e}\frac{\mathrm{Im}C^R_{II}(\omega)}{2\omega}eU$$

Zero temperature solution at particle-hole symmetry ($\mu = 0$) NFL

At zero temperature, Fermi functions reduce to step functions:

$$\mathrm{Im}C^R_{II}(\omega) = \frac{\pi e^2V^2\sqrt{NM}}{4\pi^2}\int_0^\omega d\omega_1[A(\omega_1)\mathcal{A}(\omega_1-\omega)+\mathcal{A}(\omega_1)A(\omega_1-\omega)] \quad (2.13)$$

For the NFL phase, the solutions to the saddle point equations are given by (at half filling, $n = 1/2$ or $\theta = 0$ where $p < p_c = 0.5$). Green's function G for the dot and $\mathcal{G}$ for one of the leads:

$$G_R(\omega) = \frac{\Lambda e^{-i\pi/4}}{\sqrt{J\omega}} \qquad \mathcal{G}_R(\omega) = -\sqrt{p}\frac{\sqrt{J\omega}e^{i\pi/4}}{V^2\Lambda}$$

from which we can obtain the spectral functions:

$$A(\omega) = \frac{\sqrt{2}\Lambda}{\sqrt{J|\omega|}} \qquad \mathcal{A}(\omega) = \sqrt{2p}\frac{\sqrt{J|\omega|}}{V^2\Lambda} \quad (2.14)$$

plugging these into above expression for $\mathrm{Im}C^R_{II}(\omega)$ in equation (2.13) we obtain:

$$\mathrm{Im}C^R_{II}(\omega) = \sqrt{p}e^2\sqrt{NM}\frac{1}{2\pi}\underbrace{\int_0^\omega d\omega_1\sqrt{\frac{\omega-\omega_1}{\omega_1}}+\sqrt{\frac{\omega_1}{\omega-\omega_1}}}_{\omega\pi} = \sqrt{p}e^2\sqrt{NM}\frac{1}{2}\omega$$

the current is given by:

$$\langle I(t)\rangle = \underbrace{\frac{\mathrm{Im}C^R_{II}(\omega)}{2\omega}}_{\sigma(\omega)}U = \frac{\sqrt{p}e^2\sqrt{NM}}{4}U$$

where U is the overall bias difference between two leads. Reintroducing $h = 2\pi\hbar$:

$$\boxed{\langle I(t)\rangle = \frac{\pi}{2}\sqrt{p}\sqrt{NM}\frac{e^2}{h}U}$$

Zero temperature solution at particle-hole symmetry ($\mu = 0$) FL

For the FL phase ($p > p_c = 0.5$), the Green's functions (two symmetrical leads) are found to be

$$G_R(\omega) = -\frac{it}{\sqrt{2}V^2}\frac{1}{\sqrt{2p-1}} \qquad \mathcal{G}_R(\omega) = -\frac{i}{t}\sqrt{\frac{2p-1}{2p}}$$

and the respective spectral functions

$$A(\omega) = \frac{2t}{\sqrt{2}V^2\sqrt{2p-1}} \qquad \mathcal{A}(\omega) = \frac{2}{t}\sqrt{\frac{2p-1}{2p}}$$

and as we calculate the imaginary part of the correlator using the same expression in equation (2.13)

$$\mathrm{Im}C^R_{II}(\omega) = \frac{e^2\sqrt{NM}}{\pi}\omega\frac{1}{\sqrt{p}}$$

similar to previous result in NFL phase, again reintroducing $h = 2\pi\hbar$

$$\langle I(t)\rangle = \frac{e^2}{h}\frac{1}{\sqrt{p}}\sqrt{NM}U$$

To summarize (at zero temperature), we find [17] that

$$\boxed{\langle I_{DC}\rangle = \lim_{\omega\to 0}\frac{\mathrm{Im}C(\omega)}{2\omega}U = \begin{cases}\frac{\pi}{2}\sqrt{p}\sqrt{NM}U\frac{e^2}{h} & p<0.5\\ \frac{1}{\sqrt{p}}\sqrt{NM}U\frac{e^2}{h} & p>0.5\end{cases}} \tag{2.15}$$

where U is the bias difference between one of the leads and the dot. If we define $G_0 = \sqrt{NM}\frac{e^2}{2h}$, we find that $p = 0.5$ the DC conductance of the entire system has a jump $\pi\sqrt{p}G_0 \to \frac{2}{\sqrt{p}}G_0$

Numerical Study for Linear Response Regime Conductance

In previous section we have used the conformal solutions that are obtained from the saddle point equations to evaluate the zero temperature DC conductance analytically (equation 2.15).

Now, we obtain the DC conductance using the numerical solutions of the saddle point equations (1.15) to (1.17) in DC current expression we obtained (equation 2.12). Since this is linear response regime, we also use the fluctuation dissipation relation (2.24) for both the dot and the lead Green's functions. This is where temperature enters the calculation. Strictly zero temperature is not numerically accessible since we have to use a finite value for $\beta = 1/k_BT \neq 0$. We plot the dimensionless DC conductance G/G_0 as a function of $p = M/N$. We expect to see the NFL behaviour for $p < 0.5$ separated from the FL behaviour for $p > 0.5$ by a critical point. (See the discussion in section 1.3.1)

While the FL ($p > 0.5$) regime is relatively insensitive to temperature at least below $1K$, in the NFL regime we see deviations from the zero temperature curves near the critical point $p = 0.5$ as we increase the temperature. These deviations are more pronounced at higher temperatures and closer to the critical point and they occur due to corrections that become significant as the system starts to leave the conformal regime.
Numerical solution has the advantage of accessing the entire spectrum of energies while the analytic solution [6] is valid only for low energies, bound by a critical frequency $\omega_c(p) \gg \omega$ (see equation 1.11) below which we observe conformal regime. This means that numerical solutions will include corrections to the conformal solution as we cross over to higher energies near and above $\omega_c(p)$. Note the p dependence (1.11) of $\omega_c(p)$ which vanishes (as $\sqrt{1/2-p}$) [13] as $p \to 0.5$ where we observe the strongest deviations from the conformal behaviour. In the following, we illustrate that the deviations from the analytic results in Fig. 2.1 are high energy contributions outside the conformal part of the spectral densities. Now let us go back

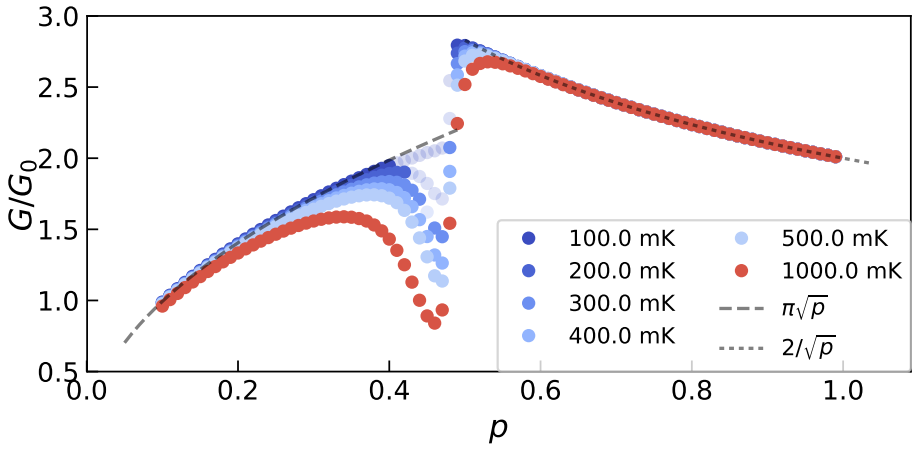

Figure 2.1: Dimensionless DC Conductance in linear response regime at various temperatures as a function of $p = M/N$ Gray dashed lines correspond to zero temperature analytic results (eqn. 2.12) We defined $G_0 = \sqrt{NM}\frac{e^2}{2h}$

to the general expression (2.12) after rearranging and writing in terms of $G_0 = \sqrt{NM}\frac{e^2}{2h}$

$$G/G_0 = \lim_{\omega\to 0} \frac{V^2}{2} \int d\omega_1 \frac{n_F(\omega_1 - \omega) - n_F(\omega_1)}{\omega} [A(\omega_1)\mathcal{A}(\omega_1 - \omega) + \mathcal{A}(\omega_1)A(\omega_1 - \omega)]$$

evaluating the limit,

$$G/G_0 = -V^2 \int d\omega_1 \partial_\omega n_F(\omega_1) A(\omega_1)\mathcal{A}(\omega_1)$$

which further reduces to the following integral after differentiating the Fermi factor:

$$G/G_0 = \beta V^2 \int d\omega_1 \frac{1}{4\cosh^2 \frac{\beta\omega_1}{2}} A(\omega_1)\mathcal{A}(\omega_1)$$

note that $(4\cosh^2 \frac{\beta\omega_1}{2})^{-1}$ is a distribution function which has the form of a peak centred at $\omega_1 = 0$ with FWHM $= 2\cosh^{-1}(2)\frac{1}{\beta} \sim \beta^{-1} \sim T$. Conformal regime, where we have analytic expressions for spectral densities [13] is observed only for frequencies $\omega \ll \omega_c$. For very low temperatures, the $1/\cosh^2$ distribution vanishes before we leave the conformal regime. However, when T becomes comparable to critical frequency ω_c as we increase temperature,

contributions from the nonconformal part of the spectal densities A and $\mathcal{A}$ in the integrand above become important and result in deviations from the conformal behaviour of the DC conductance. This departure from conformal behaviour defines a scale T^* which marks a crossover to a different regime which we explore numerically in Fig. 2.2. Notice the drastic change in the qualitative behaviour in both NFL and FL regimes. Even at very high temperatures flat curves above $p > 0.5$ can easily be distinguished by their counterparts below $p < 0.5$.

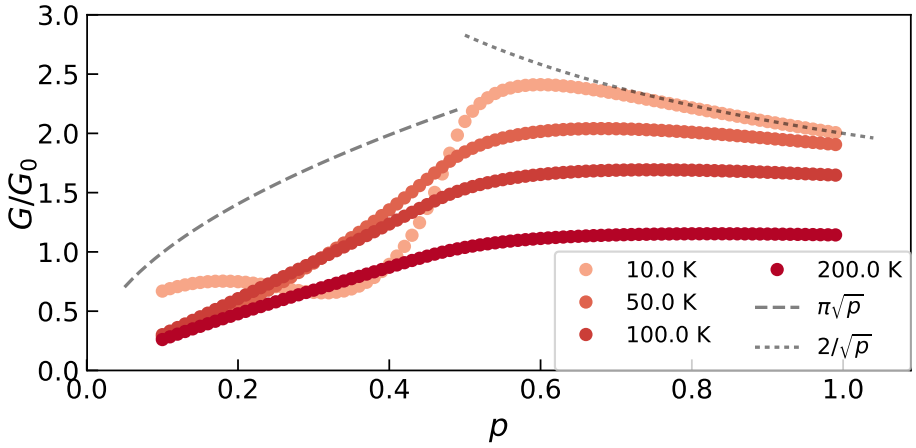

Figure 2.2: Dimensionless DC Conductance in linear response regime at temperatures above $T \gg T^*$

2.2 Experimental Considerations

In the proposed experimental setup, the main physical parameters that can be controlled are the bias voltage applied to the leads and the transverse magnetic field that is applied to the graphene flake. It is estimated that in the original realization [11] of SYK model on a graphene flake in a magnetic field, the number of SYK fermions N is estimated by

$$N = \frac{SB}{\Phi_0} = \frac{\Phi}{\Phi_0}$$

which is simply the number of flux quanta threading the graphene flake. In order to connect the results we have so far with the real experimental setup,

we relate the parameter $p = \frac{M}{N}$ to Φ/Φ_0 by eliminating N:

$$\frac{1}{p} = \frac{\Phi/\Phi_0}{M}$$

which is the number of flux quanta per lead mode where we have M of them. M can be estimated by the conductance G_{Lead} of the lead if we assume the lead has M ballistic transport channels such that $G_{\text{Lead}} = M\frac{e^2}{h}$. Therefore, if we wish to use more experimentally relevant quantities, we should plot G/G_{Lead} versus $\frac{\Phi/\Phi_0}{M}$. In this case, we can present the data in Fig. 2.1 with respect to these new parameters in Fig. 2.3.

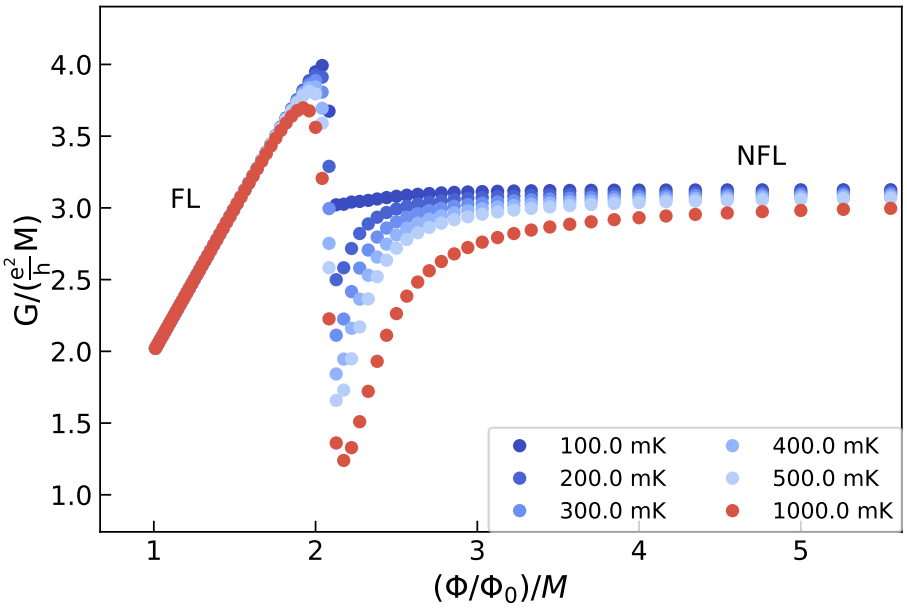

Figure 2.3: DC conductance versus the number of flux quanta per lead mode.

2.3 Weak Tunneling Regime

In this section we consider the "weak tunneling" regime where the bias voltage across the two leads can be finite. However, the coupling V between the leads and the dot must be the smallest scale in the system such that we can treat it as the perturbation with respect to the equilibrium. For simplicity, we consider the following setup: The quantum dot is at particle-hole symmetry, $\mu_D = 0$ and the lead bias voltages are symmetrically shifted

by $\pm = U/2$ such that $\mu_L = eU/2$ and $\mu_R = -eU/2$. We then turn on the coupling (2.21) provided that V is sufficiently small. (We copy the following analysis from [17])
We can use the standard tunneling conductance result ([18], Pg. 566) after Gaussian averaging the couplings V_{ij}. We can then obtain the following tunneling current formula for the weak tunneling regime:

$$\langle I(t)\rangle = 2\pi e V^2 \sqrt{NM} \int_{-\infty}^{\infty} \rho_\psi(\epsilon + eU)\rho_c(\epsilon)[n_F(\epsilon) - n_F(\epsilon + eU)]d\epsilon \quad (2.16)$$

The spectral densities we use in this formula are calculated when the leads are decoupled from the dot. The retarded Green's function of the SYK_4 model [5] at particle-hole symmetry for finite temperatures is given by:

$$G^R = \frac{-iC}{\sqrt{2\pi T}} \frac{\Gamma(1/4 - i\beta\omega/2\pi)}{\Gamma(3/4 - i\beta\omega/2\pi)}$$

We can then obtain the spectral density $\rho_c = -\frac{1}{\pi}\mathrm{Im}G^R$

$$\rho_c \propto \frac{1}{\sqrt{T}} |\Gamma(1/4 + i\beta\omega/2\pi)|^2 \cosh\left(\frac{\beta\omega}{2}\right)$$

and the Green's function for the SYK_2 model on the leads can be obtained from the retarded Green's function by setting $V = 0$ in saddle point equations and solving for the lead Green's functions:

$$\rho_\psi = \frac{1}{\pi t}\mathrm{Re}\sqrt{1 - \left(\frac{\omega}{2t}\right)^2}$$

plugging in these expressions into equation (2.16):

$$\langle I(t)\rangle \propto e\frac{V^2}{t}\sqrt{NM}\frac{1}{\sqrt{T}} \times \int_{-\infty}^{\infty} |\Gamma(1/4 + i\beta\epsilon/2\pi)|^2 \cosh\left(\frac{\beta\epsilon}{2}\right)[n_F(\epsilon) - n_F(\epsilon + eU)]d\epsilon$$

where we assumed that the lead spectral density $\rho_\psi \approx \frac{1}{\pi t}$ is flat - considering contributions only for $\epsilon \ll t$ at low energies, effectively introducing a cutoff for the integral bounds which we send to infinity, ignoring further high energy contributions. We estimate this integral in two limits:

$eU \ll k_B T$ **limit:** Fermi factors reduce to the derivative of Fermi factor

$$\lim_{\beta eU \to 0}[n_F(\epsilon) - n_F(\epsilon + eU) = \frac{\beta eU}{4\cosh^2(\beta\epsilon/2)}$$

the integral above becomes:

$$\langle I_{WT}) \rangle \propto e\frac{V^2}{t}\sqrt{NM}\frac{1}{\sqrt{T}}eU\int_{-\infty}^{\infty}\frac{|\Gamma(1/4 + i\beta\epsilon/2\pi)|^2}{4\cosh(\beta\epsilon/2)}d(\beta\epsilon)$$

Note that the integral reduces to a dimensionless constant. Then, from this expression we can easily extract the dependence to the external parameters of the model.

$$\langle I_{WT} \rangle \propto \frac{eU}{\sqrt{T}} \quad (eU \ll k_B T) \tag{2.17}$$

$eU \gg k_B T$ **limit:** Fermi factors introduce limits to the integral this time, as they are effectively step functions at temperatures much smaller than bias voltage:

$$\langle I(t) \rangle \propto e\frac{V^2}{t}\sqrt{NM}\frac{1}{\sqrt{T}}\frac{1}{\beta}\int_{-\beta eU}^{0}|\Gamma(1/4 + i\beta\epsilon/2\pi)|^2\cosh\left(\frac{\beta\epsilon}{2}\right)d(\beta\epsilon)$$

for $\beta\epsilon \gg 1$ the integrand can be estimated as the following:

$$|\Gamma(1/4 + i\beta\epsilon/2\pi)|^2\cosh\left(\frac{\beta\epsilon}{2}\right) \sim \frac{1}{\sqrt{|\beta\epsilon|}}$$

then the integral can be estimated as

$$\langle I_{WT} \rangle \propto e\frac{V^2}{t}\sqrt{NM}\frac{1}{\sqrt{\beta T}}\sqrt{eU}$$

from which we can extract the dependencies to external parameters:

$$\langle I(t) \rangle \propto \sqrt{eU} \quad (eU \gg k_B T) \tag{2.18}$$

It is important to recall that we assumed $\omega \ll t$ above, which that the results that we have should be valid only when temperature and the bias is much smaller than t. To summarize our results for the weak tunneling regime, we found that the weak tunneling current I_{WT} is given by

$$\boxed{\langle I_{WT} \rangle \propto \begin{cases} eU/\sqrt{T} & (eU \ll k_B T) \\ \sqrt{eU} & (eU \gg k_B T) \end{cases}} \tag{2.19}$$

We can also read off the tunneling conductance from these results:

$$\boxed{G(U) \propto \begin{cases} 1/\sqrt{T} & (eU \ll k_B T) \\ 1/\sqrt{U} & (eU \gg k_B T) \end{cases}} \tag{2.20}$$

Note the non-linear behaviour at temperatures much lower than the bias voltage across the leads.

In next section, we will derive a more general formula (2.22) for the current which is valid even when we are far from equilibrium. After obtaining the general formula, we show that the numerical results we obtain with it reduces to the dependencies (2.19) near equilibrium.

2.4 Beyond Equilibrium

In this section we obtain a general expression for the current between two sites where the coupling between the two is given by

$$H_{c\psi} = \frac{1}{(NM)^{1/4}} \sum_{ij} V_{ij} c_i^\dagger \psi_j + V_{ij}^* \psi_j^\dagger c_i \tag{2.21}$$

where the couplings V_{ij} are drawn from a random Gaussian distribution with the variance $\overline{|V_{ij}|^2} = V^2$. We have used the Keldysh formalism to address nonequilibrium transport where the bias voltage between two sites can be finite. The derivation given in detail can be found in the appendix A.3. The general expression for net current from the left lead (ψ_L operators) to the quantum dot (c operators) is given by

$$\langle I_{LD} \rangle = ie\sqrt{NM}V^2 \int d\omega \left\{ G^<(\omega)\mathcal{A}_L(\omega) - \mathcal{G}_L^<(\omega)A(\omega) \right\} \tag{2.22}$$

Where G and $\mathcal{G}_L$ are the correlators associated with c and ψ_L respectively. The Green's functions enter this formula must be calculated in the presence of couplings between sites. This formula is valid in large-N, M saddle point approximation. Similarly, we could define the current from the quantum dot to the right lead (ψ_R operators)

$$\langle I_{DR} \rangle = ie\sqrt{NM}V^2 \int d\omega \left\{ \mathcal{G}_R^<(\omega)A(\omega) - G^<(\omega)\mathcal{A}_R(\omega) \right\} \tag{2.23}$$

In steady state, where there is no charge accumulation on the quantum dot, the net current $\langle I \rangle$ through the entire junction must be $\langle I \rangle = \langle I_{LD} \rangle = \langle I_{DR} \rangle$.

This is the statement of current conservation which we will address shortly in section 2.4.3 We assume that the ψ_L and ψ_R degrees of freedom, fermionic modes at the endpoints of the left and right leads respectively, which are the SYK_2 models of the tips of the leads are in equilibrium with reservoirs. However, we do not assume equilibrium for the graphene flake quantum dot, which we take to be at zero chemical potential. We symmetrically shift the chemical potentials of the leads by $\pm\mu/2$ where $\mu = eU$ where U is the potential difference between two leads, across the entire system. *In the following analysis we ignore the effect of the reservoirs on the leads except that the reservoirs determine the thermal distribution functions for the leads. In section 2.5, we will justify this assumption.* Since the leads are in equilibrium as they are in contact with reservoirs, we can impose the FDT condition on the leads Green's functions. We assume that the left lead has the higher potential:

$$\mathcal{G}^K_{L/R}(\omega) = 2i \tanh\left(\frac{\beta(\omega \pm \mu/2)}{2}\right) \mathrm{Im}\mathcal{G}^R_{L/R}(\omega). \tag{2.24}$$

With these assumptions, we compute the current (2.22) as a function of applied bias in the next section for linear response regime and weak tunneling regime.

2.4.1 I-V characteristics in Weak-Tunneling Regime

In weak tunneling regime which we introduced in section 2.3, we studied the the tunneling current I_{WT} in two different limits. While it is proportional to $eU/\sqrt{T}$ for $eU \ll k_BT$, in $eU \gg k_BT$ limit it shows $\sqrt{eU}$ dependence. In this section, we will match these near equilibrium weak-tunneling results to the current computed with the formula (2.22) using the numerical solutions of the saddle point equations (1.15-1.17) in the weak tunneling regime where we take V to be sufficiently small. Here we take $t = J/2$, $V = 0.025J$ and $p = 0.3$. First we consider the high bias regime ($eU \gg k_BT$). (See Fig. 2.4(a)) Note that in high bias regime I-V curves do not depend on temperature and agree with the analytical prediction $I \propto \sqrt{eU/J}$ (2.19) up to $eU \sim 0.1J$. At low biases, we observe a temperature dependent behaviour yet it is linear in applied bias. In Fig. 2.4(b) we plot $I\sqrt{T}$ versus eU to observe the scaling collapse that occurs for $I \propto eU/\sqrt{T}$ at low bias regime ($eU \ll k_BT$)

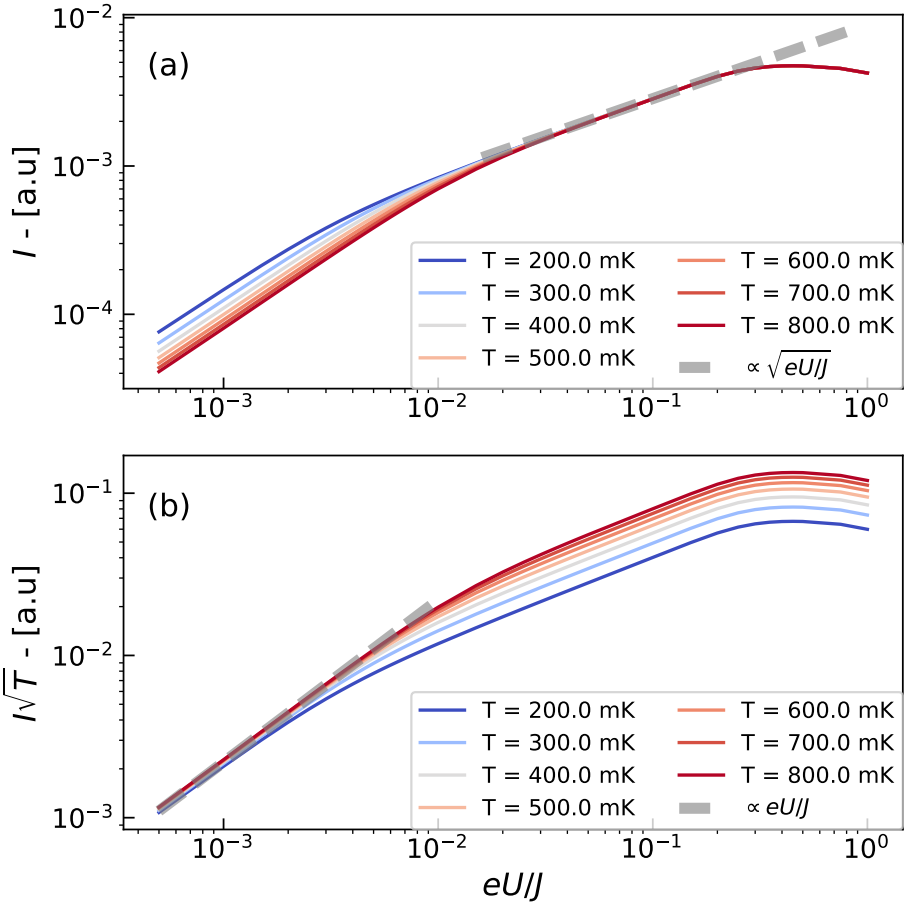

Figure 2.4: I-V characteristics in the weak tunneling regime for various temperatures. Numerical results are shown in solid curves. In high bias regime $eU \gg k_B T$ we find that the current calculated with (2.22) using numerical solutions of the saddle point equations matches weak tunneling analytical prediction (2.19) $I\sqrt{T}$ - eU/J characteristics in the weak tunneling regime for various temperatures. For low bias regime $eU \ll k_B T$ we observe a scaling collapse, confirming the predicted $eU/\sqrt{T}$ dependence

2.4.2 I-V characteristics in Linear Response Regime

Using the numerical solutions of the saddle point equations with the assumptions described above, we compute the current as a function of applied bias. We plot the $I-V$ characteristics of the system in Fig. 2.5. Notice the linear behaviour at very low values of bias eU/J. The current curves are normalized by a $1/\sqrt{p}$ factor and for sufficiently low values of bias all curves tend to collapse to a single line, suggesting that current has $\sqrt{p}$ dependence, which is in agreement with the linear response regime results (2.15). As the

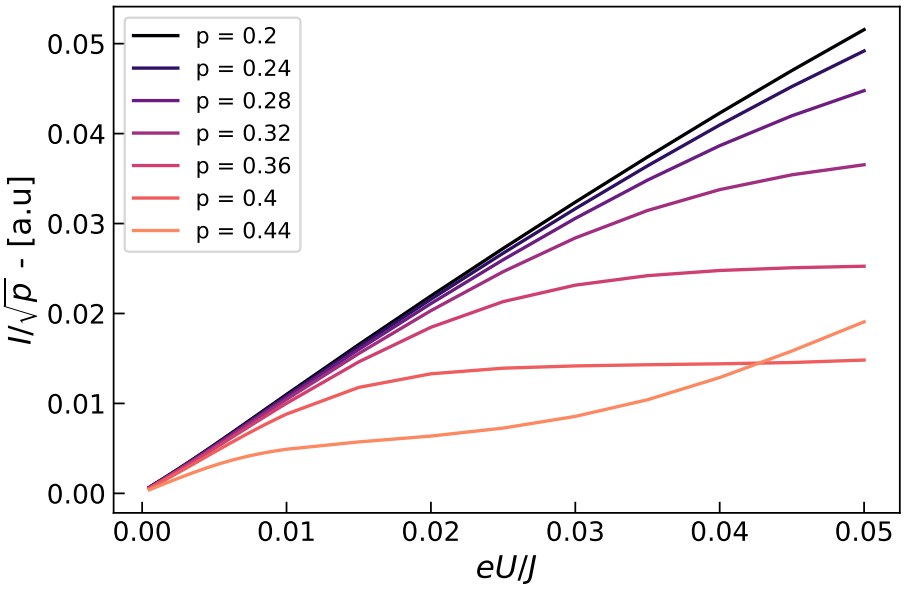

Figure 2.5: DC current versus bias voltage eU at steady state transport in arbitrary units for T= 400mK and various values of $p = M/N < 0.5$ in the NFL regime

bias eU is increased, the curves depart from the linear response regime. The onset of nonlinear regime begins relatively earlier as we get closer to the phase transition $p \to 0.5$ whereas deep in the NFL phase (near $p = 0.2$) we see linear $I-V$ characteristics up to roughly $eU = 0.025J$

We plot the current in Fig 2.6 as a function of p for various bias values up to $eU \sim J$ such that we can observe the how the current evolves as we depart from the linear response regime as a function of p. The lowest bias that we show is $eU = 0.006J$. For the same bias value, we project

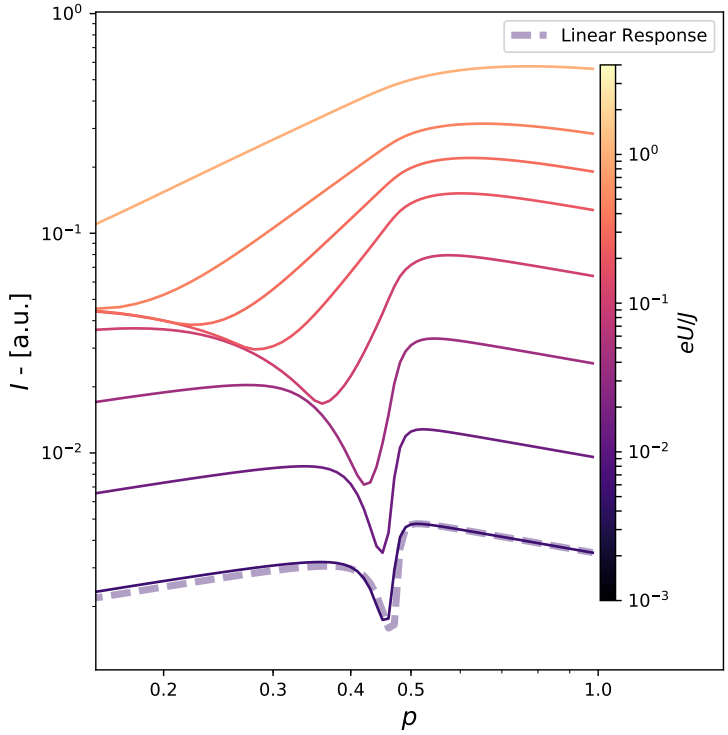

Figure 2.6: DC current at steady state transport in arbitrary units for T= 400mK. Solid curves correspond to various bias voltages U across two leads. The dashed curve shows the linear response current projected to $eU = 0.006J$ from the DC conductance G we have calculated numerically using (2.12)

the linear response current (dashed curve) from the DC conductance we have computed numerically in section 2.1. This shows that the formula (2.22) captures the linear response regime. We can now increase bias eU and study the departures from the linear response regime. The lowest three curves (the third one corresponds to $eU = 0.04J$) show that while the FL part ($p > 0.5$) is unaffected, the range of p values below which we see the $\sqrt{p}$ dependence shrinks until we crossover to a different regime at higher biases at order $eU \sim J$ where the p dependence of current is very similar to high temperature linear response behaviour (Fig. 2.2) we obtained near equilibrium.

2.4.3 Current conservation

In steady state transport, there should not be any charge accumulation on the dot. This means that the current between the left lead and the dot I_{LD} is equal to the current between the dot and the right lead I_{DR}. The current conservation

$$I_{LD} = I_{DR}$$

then implies when we incorporate the equation (2.22) into this equality:

$$\int d\omega \left\{ G^<(\omega)\mathcal{A}_L(\omega) - \mathcal{G}_L^<(\omega)A(\omega) \right\} = \int d\omega \left\{ \mathcal{G}_R^<(\omega)A(\omega) - G^<(\omega)\mathcal{A}_R(\omega) \right\}$$

which can be rearranged as

$$\int d\omega \left\{ G^<(\omega)(\mathcal{A}_L(\omega) + \mathcal{A}_R(\omega)) - (\mathcal{G}_L^<(\omega) + \mathcal{G}_R^<(\omega))A(\omega) \right\} = 0 \qquad (2.25)$$

This is the statement of current conservation and does not depend on the specifics of the system apart from the random Gaussian form of coupling (2.21) we have defined in the large-N, M limit. It can be shown, for our model, that in the saddle point approximation a stronger statement could be made than equation (2.25). Combining the saddle point equations (1.15-1.17) with the Keldysh equation $G^< = G^R\Sigma^<G^A$ which follows from the Dyson's equation in Keldysh formalism, it can be shown that not only the equation (2.25) holds but also the integrand is zero for all frequencies [17]. Then we obtain the following form for the $G^<$:

$$G^<(\omega)(\mathcal{A}_L(\omega) + \mathcal{A}_R(\omega)) = (\mathcal{G}_L^<(\omega) + \mathcal{G}_R^<(\omega))A(\omega) \qquad (2.26)$$

since we assume that the leads are in equilibrium with reservoirs, they follow the distributions:

$$f_L(\omega) = \frac{1}{e^{\beta\omega + eU/2} + 1} \quad \text{and} \quad f_R(\omega) = \frac{1}{e^{\beta\omega - eU/2} + 1} \qquad (2.27)$$

at half filling $\mu = 0$. And in equilibrium for the leads, we can combine $\mathcal{G}^{<}_{L/R} = if_{L/R}(\omega)\mathcal{A}_{L/R}$ with equation (2.26) to obtain a distribution form for the dot green's function G which is not in equilibrium:

$$G^{<}(\omega) = i\frac{f_L(\omega)\mathcal{A}_L(\omega) + f_R(\omega)\mathcal{A}_R(\omega)}{\mathcal{A}_L(\omega) + \mathcal{A}_R(\omega)}A(\omega) \tag{2.28}$$

This is the statement of current conservation. We use this condition on the dot Green's function G when we solve the saddle point equations (1.15-1.17) numerically.

2.5 Coupling to Reservoirs

In our analysis we have assumed that the lead endpoints are in equilibrium with reservoirs but we have so far ignored the effect of the reservoirs on the leads even though the lead endpoints must be strongly coupled to the reservoirs so that we can assume equilibrium forms (2.27) for the lead endpoints. When the extended leads are ignored we have M fermionic modes which constitute the SYK_2 models on the lead endpoints which are coupled to the dot via equation (2.21). To introduce the effect of the reservoirs, one can couple the reservoirs to the lead endpoints (where the SYK_2 lives) with semi-infinite noninteracting 1D ballistic chains. (See SM for reference [17]). This coupling can be taken into account by renormalizing the bare lead propagators [17] $\mathcal{G}^0_L$ and $\mathcal{G}^0_R$ (this is shown in equilibrium, therefore one can work in Matsubara formalism which can then be incorporated into Keldysh equations in equilibrium):

$$\mathcal{G}^0_{L/R}(i\omega_n) \to \mathcal{G}^0_{L/R}(i\omega_n) - \Sigma_{E(L/R)}(i\omega_n)$$

where, after analytic continuation, retarded self energy $\Sigma^R_{E(L/R)}$ is given by:

$$\Sigma^R_{E(L/R)} = \rho_E t_E^2 \ln\left|\frac{\omega + D}{\omega - D}\right| - i\pi\rho_E t_E^2$$

where t_E is the coupling of the 1D chains to the lead endpoints, ρ_E is local density of states at the end of leads and $D \ll J$ is a cutoff of the order of the lead bandwidths. Once we have the retarded self energy $\Sigma^R_{E(L/R)}$ for both leads, we can write it a s in Keldysh basis and update the bare lead endpoint propagators in Dyson equations (1.18-1.20) as following:

$$\sigma^z\left(\omega + \mu\right) \to \sigma^z\left(\omega + \mu\right) - \Sigma^w_{L/R}(\omega)$$

therefore, taking the corrections due to coupling to the extended leads into account. Now we can solve the updated saddle point equations numerically and compare the solutions where we considered the coupling to reservoirs with the earlier solutions where we have ignored it. In Fig. 2.7 we consider the spectral functions of the dot and the left lead in the same plot for various values of $\rho_E t_E^2$, in equilibrium.

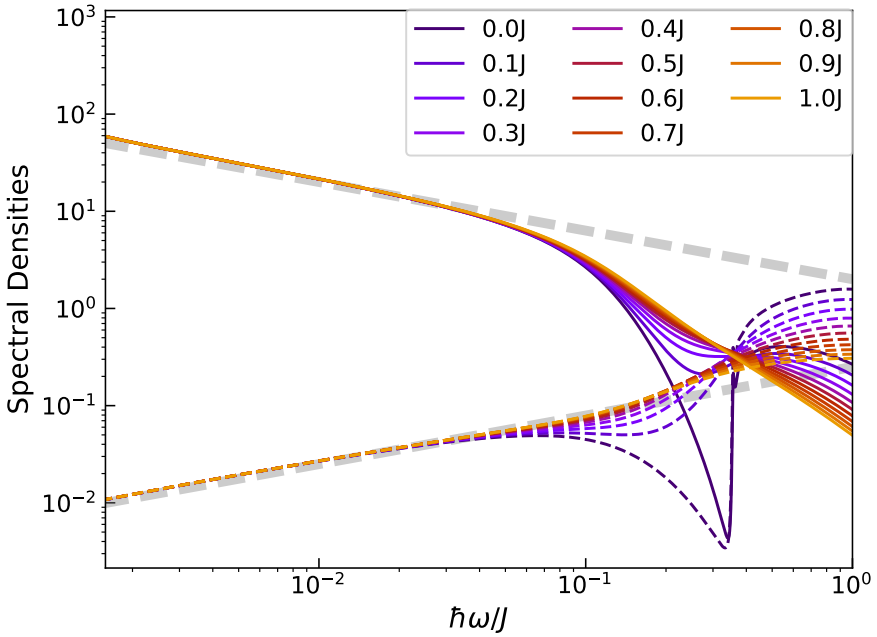

Figure 2.7: Spectral functions of the dot (solid lines) and the left lead (dashed lines) for various values of $\rho_E t_E^2$ in units of J in equilibrium, $p = 0.1$ The low energy behaviour is unaffected (up to $\rho_E t_E^2 \sim J$) by the coupling of the lead endpoints to the semi-infinite wires coupling the system to the reservoirs. In conformal regime, dot and the lead spectral functions show $\omega^{-1/2}$ and $\omega^{1/2}$ dependence (2.14) respectively. This conformal behaviour is outlined by grey dashed lines.

We tune the coupling t_E from 0 to $t_E \sim \sqrt{J/\rho_E}$. ($t = V = J/2$, in equilibrium) Notice that the low energy spectrum where we see the conformal behaviour is robust in the presence of coupling to semi infinite wires. Since the transport quantities we have considered so far depend on low energy features of the spectral functions at low temperatures, we therefore expect

to see similar transport behaviour when we actually couple the system to the reservoirs.

Now consider the case where we turn off the disorder, completely ignoring the SYK_2 part at the endpoints of the leads and still couple the SYK_4 dot to the semi-infinite wires with random couplings (2.21). This can be achieved by setting $V = J/2$ as before, but $t = 0$ then turn on t_E which is the coupling of the lead endpoints to the rest of the semi-infinite wire (Fig. 2.8) Even

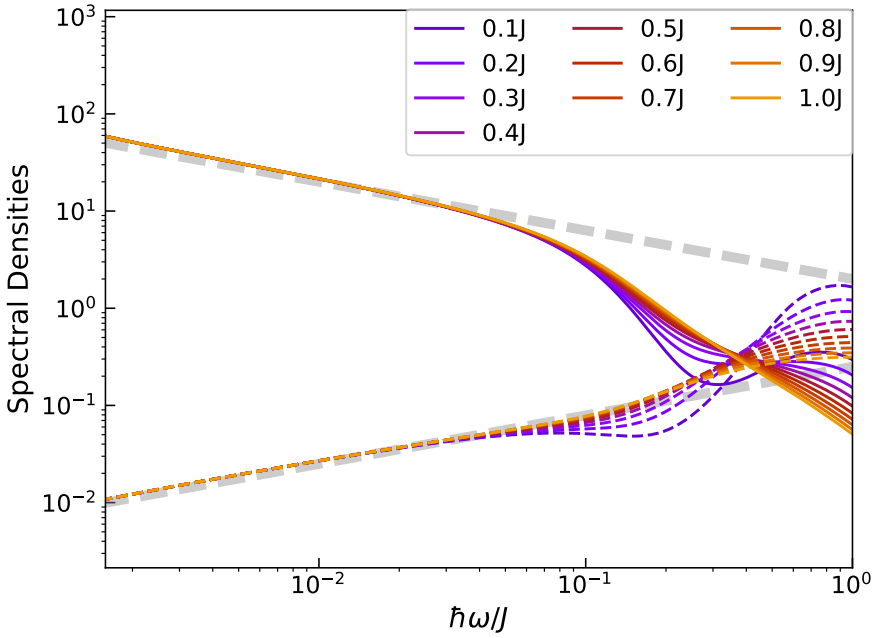

Figure 2.8: Spectral functions of the dot (solid lines) and the left lead (dashed lines) for various values of $\rho_E t_E^2$ in units of J in equilibrium, $p = 0.1$, in the absence of SYK_2 ($t = 0$) at the lead endpoints. The low energy behaviour is the same (compare to Fig. 2.7), regardless of whether disorder is present at the lead endpoints.

if we completely ignore disorder at the lead endpoints, we find that the conformal low energy behaviour is the same as BA [13] model. We can also consider the linear response conductance results which we computed earlier in Fig. 2.1. We compare three cases where the system is completely decoupled from the reservoirs (Fig. 2.9a), coupled to reservoirs (Fig. 2.9b) and finally, the case where there is no disorder at the lead endpoints ($t = 0$)

but the system is coupled to the reservoirs (Fig. 2.9c) We use the same model paramters as above, but $t_E = \sqrt{J/2\pi\rho_E}$ when the system is coupled to the reservoirs. See Fig.2.9 for comparison of DC conductances as functions of p in these three cases we described above. We observe the same qualitative behaviour in all three cases away from the critical point $p_c = 0.5$, justifying our assumption of ignoring the explicit coupling to the reservoirs. Note that the deviations from the conformal behaviour near the critical point is weaker in the presence of coupling to the reservoirs (Figs. 2.9b and 2.9c) in comparison to the isolated model (Fig. 2.9a) we started with.

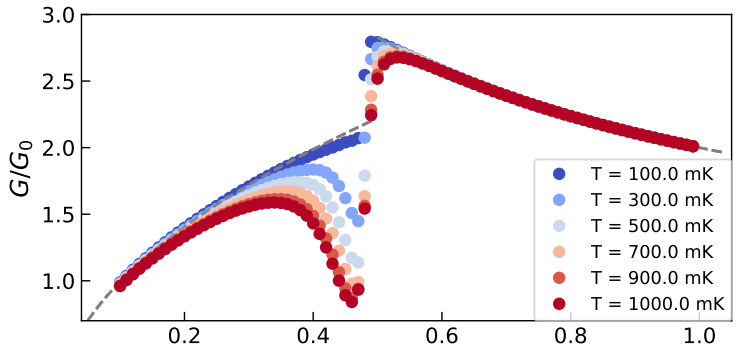

(a) Decoupled from reservoirs, ($t = V = J/2$)

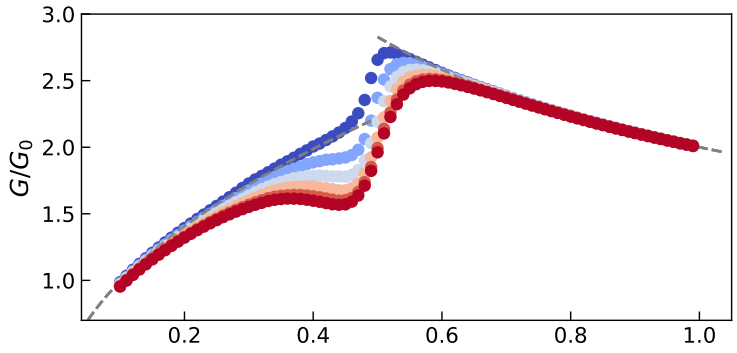

(b) Coupled to reservoirs, ($t = V = J/2$)

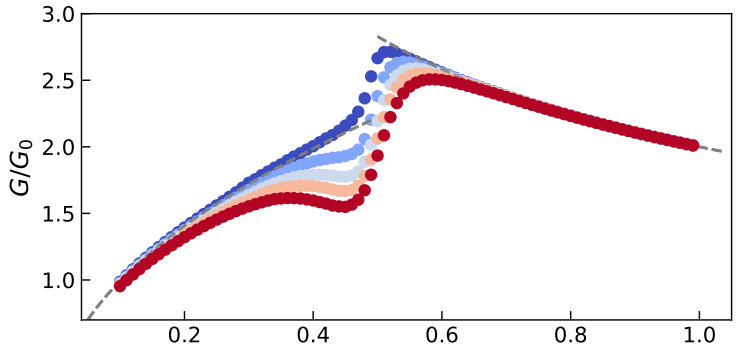

(c) Coupled to reservoirs, no disorder at the lead endpoints ($V = J/2$, $t = 0$)

Figure 2.9: DC conductance as a function of p. We consider the effects of coupling to the reservoirs $t_E = \sqrt{J/2\pi\rho_E}$ and the presence of disorder t at the lead endpoints

Chapter 3

Summary and Conclusion

We have explored the charge transport signatures of the SYK model.Starting with the "linear response" (section 2.1) and the "weak tunneling" (section 2.3) regimes near equilibrium, we then bridged these two approaches with a more general formula (A.34) we have derived which is valid in and beyond equilibrium at finite bias voltage across the leads. Although we have used this formula for the specific model we studied in this work, the derivation of the current expression for large-N at saddle point approximation did not depend on the specific details of the model except for the form of coupling (2.21) between two sites between which we consider the current. The formula is valid as long as the two sites we consider for transport admit large-N "classical" saddle point solutions as SYK model does. For instance, the same formula can be used to study nonequilibrium transport properties of a chain of SYK models which are coupled via the form (2.21).

In linear response regime, at low temperatures, we observed a jump (see Figs. 2.1 and 2.3) in tunneling conductance as we tune the magnetic field threading the flake. This jump corresponds to an experimental signature of the NFL-FL transition proposed in the Banerjee-Altman model [13]. As we increase the temperature, we find that the jump disappears and we see a crossover to a high temperature (Fig. 2.2) regime where the remnants of the NFL-FL transition at zero temperature can still be seen.

Weak tunneling regime allows us to study the current-bias characteristics at finite biases within the linear response framework. We have found [17] (2.20) that in the NFL regime at temperatures much lower than the bias voltage, tunneling conductance $G \propto U^{-1/2}$ is highly nonlinear and does not depend on temperature. At higher temperatures, conductance $G \propto T^{-1/2}$ becomes ohmic and exhibits temperature dependence.

Using the general current formula (A.34), we have computed the current-bias curves (Fig. 2.6) for finite bias voltage values up to order J. We find that the jump that we have seen in linear response regime disappears and we observe a crossover to a high bias regime where the I-V characteristics are very similar to the high temperature regime I-V characteristics of the linear response regime at infinitesimal bias across the two leads.

We have also considered the effect of the reservoirs on the transport signatures of the SYK model and shown numerically that the low energy behaviour is unaffected (Fig. 2.7) by explicit coupling of the lead endpoints to featureless extended wires which are modeled as the reservoirs, justifying our inital assumption of considering only the lead endpoints (assumed to be decoupled from, yet in equilibrium with the reservoirs) which are generically modified by explicit coupling to reservoirs.

To summarize, we have proposed a relatively simple transport experiment and computed directly measurable quantities displaying signatures of SYK physics. We believe that the graphene flake realization [11], through such an experiment, would open up more possibilities for further exploration of the SYK model in a laboratory setting, confirm theoretical predictions and possibly help us overcome the difficulties we encounter using numerical and theoretical techniques.

Bibliography

[1] Alexei Kitaev. A simple model of quantum holography. *talk given at KITP*, Apr 2015.

[2] Juan Maldacena and Douglas Stanford. Remarks on the sachdev-ye-kitaev model. *Phys. Rev. D*, 94:106002, Nov 2016.

[3] Juan Maldacena, Stephen H. Shenker, and Douglas Stanford. A bound on chaos. *Journal of High Energy Physics*, 2016(8):106, Aug 2016.

[4] Subir Sachdev. Holographic metals and the fractionalized fermi liquid. *Phys. Rev. Lett.*, 105:151602, Oct 2010.

[5] Subir Sachdev. Bekenstein-hawking entropy and strange metals. *Phys. Rev. X*, 5:041025, Nov 2015.

[6] Subir Sachdev and Jinwu Ye. Gapless spin-fluid ground state in a random quantum heisenberg magnet. *Phys. Rev. Lett.*, 70:3339–3342, May 1993.

[7] S.A. Hartnoll, A. Lucas, and S. Sachdev. *Holographic Quantum Matter*. The MIT Press. MIT Press, 2018.

[8] Ippei Danshita, Masanori Hanada, and Masaki Tezuka. Creating and probing the sachdevyekitaev model with ultracold gases: Towards experimental studies of quantum gravity. *Progress of Theoretical and Experimental Physics*, 2017(8):083I01, 2017.

[9] D. I. Pikulin and M. Franz. Black hole on a chip: Proposal for a physical realization of the sachdev-ye-kitaev model in a solid-state system. *Phys. Rev. X*, 7:031006, Jul 2017.

[10] Aaron Chew, Andrew Essin, and Jason Alicea. Approximating the sachdev-ye-kitaev model with majorana wires. *Phys. Rev. B*, 96:121119, Sep 2017.

[11] Anffany Chen, R. Ilan, F. de Juan, D. I. Pikulin, and M. Franz. Quantum holography in a graphene flake with an irregular boundary. *Phys. Rev. Lett.*, 121:036403, Jul 2018.

[12] Marcel Franz and Moshe Rozali. Mimicking black hole event horizons in atomic and solid-state system. *ArXiv e-prints, arXiv:1808.00541 [cond-mat]*, Aug 2018.

[13] Sumilan Banerjee and Ehud Altman. Solvable model for a dynamical quantum phase transition from fast to slow scrambling. *Phys. Rev. B*, 95:134302, Apr 2017.

[14] Xue-Yang Song, Chao-Ming Jian, and Leon Balents. Strongly correlated metal built from sachdev-ye-kitaev models. *Phys. Rev. Lett.*, 119:216601, Nov 2017.

[15] Wenbo Fu and Subir Sachdev. Numerical study of fermion and boson models with infinite-range random interactions. *Phys. Rev. B*, 94:035135, Jul 2016.

[16] A. Kamenev and A. Levchenko. Keldysh technique and non-linear σ-model: basic principles and applications. *Advances in Physics*, 58:197–319, May 2009.

[17] Oguzhan Can, Emilian M. Nica, and Marcel Franz. Charge transport in graphene-based mesoscopic realizations of Sachdev-Ye-Kitaev models. *ArXiv e-prints, arXiv:1808.06584 [cond-mat]*, Aug 2018.

[18] Gerald D. Mahan. *Many-particle Physics, 3rd Edition*. Plenum, New York, 2000.

[19] Yigal Meir and Ned S. Wingreen. Landauer formula for the current through an interacting electron region. *Phys. Rev. Lett.*, 68:2512–2515, Apr 1992.

[20] Hartmut J. W. Haug and Anti-Pekka Jauho. *Quantum Kinetics in Transport and Optics of Semiconductors*. Springer-Verlag, Berlin, 2008.

Appendix A

Saddle Point Calculations

A.1 Keldysh Action

Following Ref. [14], we write down the path integral for equations 1.1-1.3, ignoring the extended leads, and obtain an effective action after disorder averaging

$$\overline{Z} = \int \mathcal{D}\left[\psi, \overline{\psi}, c, \overline{c}\right] e^{iS}, \tag{A.1}$$

where the Grassmann fields ψ, c correspond to a lead endpoint and the dot, respectively. We work with only one lead for simplicity since both leads are identical. The other lead will be introduced at the end of the calculation. The real-time action is defined on the Keldysh contour and can be written as a sum of contributions from the lead, dot, and coupling between them:

$$S = S_L + S_D + S_{LD} \tag{A.2}$$

$$\begin{aligned} S_L &= \sum_s \sum_\alpha \int dt \left\{ \overline{\psi}_{\alpha s}(t) s \left[i\partial_t + \mu \right] \psi_{\alpha s}(t) \right\} \\ &- \sum_{ss'} \int\int dt dt' \left\{ ss' \frac{it^2}{2M} \left(\sum_\alpha \overline{\psi}_{\alpha s}(t) \psi_{\alpha s'}(t') \right) \left(\sum_\beta \overline{\psi}_{\beta s'}(t') \psi_{\beta s}(t) \right) \right\} \end{aligned}$$

$$\begin{aligned} S_D &= \sum_s \sum_i \int dt \left\{ \overline{c}_{is}(t) s \left[i\partial_t + \mu \right] c_{is}(t) \right\} \\ &+ \sum_{ss'} \int\int dt dt' \left\{ ss' \frac{iJ^2}{4N^3} \left(\sum_i \overline{c}_{is}(t) c_{is'}(t') \right)^2 \left(\sum_j \overline{c}_{js'}(t') c_{js}(t) \right)^2 \right\} \end{aligned}$$

(A.3)

$$S_{LD} = -\sum_{ss'} \int\int dtdt' \left\{ ss' \frac{iV^2}{\sqrt{NM}} \left(\sum_i \overline{c}_{is}(t) c_{is'}(t') \right) \left(\sum_\alpha \overline{\psi}_{\alpha s'}(t') \psi_{\alpha s}(t) \right) \right\}. \tag{A.4}$$

The integrals run from $-\infty$ to ∞ and the index $s = \pm 1$ labels the forward and backward direction on the Keldysh contour. We introduce the fields G and $\mathcal{G}$ together with the Lagrange multipliers $\Sigma^{c,\psi}$:

$$\int \mathcal{D}[G, \Sigma^c] e^{N \sum_{ss'} \int\int dtdt' \Sigma^c_{ss'}(t,t') \left[G_{s's}(t',t) - \frac{i}{N} \sum_i \overline{c}_{is}(t) c_{is'}(t') \right]} = 1$$

$$\int \mathcal{D}[\mathcal{G}, \Sigma^\psi] e^{M \sum_{ss'} \int\int dtdt' \Sigma^\psi_{ss'}(t,t') \left[\mathcal{G}s's(t',t) - \frac{i}{M} \sum_i \overline{\psi}_{is}(t) \psi_{is'}(t') \right]} = 1.$$

The resulting action is

$$\begin{aligned} S_L = & \sum_{ss'} \sum_\alpha \int\int dtdt' \left\{ \overline{\psi}_{\alpha s}(t) \left[\sigma^z_{ss'} \delta_{tt'} \left(i\partial_t + \mu \right) - \Sigma^\psi_{ss'}(t,t') \right] \psi_{\alpha s'}(t') \right\} \\ & + \sum_{ss'} \int\int dtdt' \left\{ iss' \frac{Mt^2}{2} \mathcal{G}_{s's}(t',t) \mathcal{G}_{ss'}(t,t') - iM \Sigma^\psi_{ss'}(t,t') \mathcal{G}_{s's}(t',t) \right\} \end{aligned}$$

$$\begin{aligned} S_D = & \sum_{ss'} \sum_i \int\int dtdt' \left\{ \overline{c}_{is}(t) \left[\sigma^z_{ss'} \delta_{tt'} \left(i\partial_t + \mu \right) - \Sigma^c_{ss'}(t,t') \right] c_{is'}(t') \right\} \\ & + \sum_{ss'} \int\int dtdt' \left\{ iss' \frac{NJ^2}{4} G^2_{s's}(t',t) G^2_{ss'}(t,t') - iN \Sigma^c_{ss'}(t,t') G_{s's}(t',t) \right\} \end{aligned}$$

$$S_{LD} = \sum_{ss'} \int\int dtdt' \left\{ iss' \sqrt{NM} V^2 G_{s's}(t',t) \mathcal{G}_{ss'}(t,t') \right\}$$

After integrating out fermions, we find the saddle point of the action

$$\frac{\delta S}{\delta G_{ss'}(t,t')} = 0, \qquad \frac{\delta S}{\delta \mathcal{G}_{ss'}(t,t')} = 0 \tag{A.5}$$

$$\frac{\delta S}{\delta \Sigma^c_{ss'}(t,t')} = 0, \qquad \frac{\delta S}{\delta \Sigma^\psi_{ss'}(t,t')} = 0 \tag{A.6}$$

Dropping the dependence on two time indices, we obtain the saddle-point equations which follow from equations (A.5)

$$\Sigma^c_{ss'}(t) = ss' J^2 G^2_{ss'}(t) G_{s's}(-t) + ss'\sqrt{p} V^2 \mathcal{G}_{ss'}(t) \tag{A.7}$$

$$\Sigma^\psi_{ss'}(t) = ss' t^2 \mathcal{G}_{ss'}(t) + ss' \frac{V^2}{\sqrt{p}} G_{ss'}(t), \tag{A.8}$$

where $p = M/N$. These are supplemented by the (matrix) Dyson equation for the frequency-dependent Green's functions which we obtain from (A.6)

$$G_{ss'}(\omega) = \left[\sigma^z(\omega + \mu) - \Sigma^c\right]^{-1}_{ss'} \tag{A.9}$$

$$\mathcal{G}_{ss'}(\omega) = \left[\sigma^z(\omega + \mu) - \Sigma^\psi\right]^{-1}_{ss'} \tag{A.10}$$

These equations can easily be generalized to the case where there are two separate flavours of ψ operators corresponding to left and right leads. We need to add a third term to (A.7) similar to its second term (to introduce the other lead) and write down another self energy equation similar to (A.8) as well as a separate Dyson's equaiton for this new fermion flavour we introduced. The final result is given by (1.15-1.17)

A.2 Linear Response at Saddle Point

We need to evaluate the time contour correlator

$$C_{II}(\tau_1, \tau_2) = -i\langle \hat{T}_C I(\tau_1) I(\tau_2)\rangle$$

which can then be analytically continued to the retarded correlation function $C^R_{II}(\omega)$. Plugging in the expression for current operator in equation (2.2), we obtain the following (we suppress the denominator in $V_{ij} = V_{ij}/(NM)^{1/4}$)

$$\begin{aligned} C_{II}(\tau_1, \tau_2) = ie^2 \sum_{ijkl} & V_{ij} V_{kl} \langle \hat{T} c^\dagger_i(\tau_1) d_j(\tau_1) c^\dagger_k(\tau_2) d_l(\tau_2)\rangle \\ & - V_{ij} V^*_{kl} \langle \hat{T} c^\dagger_i(\tau_1) d_j(\tau_1) d^\dagger_l(\tau_2) c_k(\tau_2)\rangle \\ & - V^*_{ij} V_{kl} \langle \hat{T} d^\dagger_j(\tau_1) c_i(\tau_1) c^\dagger_k(\tau_2) d_l(\tau_2)\rangle \\ & + V^*_{ij} V^*_{kl} \langle \hat{T} d^\dagger_j(\tau_1) c_i(\tau_1) d^\dagger_l(\tau_2) c_k(\tau_2)\rangle \end{aligned} \tag{A.11}$$

We can evaluate these correlators in path integral formalism (Keldysh contour) at the saddle point. Let us compute one of these terms explicitly as

the others will follow similarly. For instance, consider the third term in the above expression. In time-contour path integral formalism, we can write:

$$
\begin{aligned}
&-ie^2 \sum_{ijkl} V_{ij}^* V_{kl} \langle \hat{T} d_j^\dagger(\tau_1) c_i(\tau_1) c_k^\dagger(\tau_2) d_l(\tau_2) \rangle \\
&= -ie^2 \sum_{ijkl} \int \mathcal{D}[c,d] e^{iS_c + iS_d} \overline{d}_{j\tau_1} c_{i\tau_1} \overline{c}_{k\tau_2} d_{l\tau_2} V_{ij}^* V_{kl} e^{\sum_{ij} \phi_{ij} V_{ij} + \phi_{ij}^* V_{ij}^*}
\end{aligned} \tag{A.12}
$$

where S_c and S_d are the Keldysh actions for c and d fermions. We wrote the coupling term separately, with the shorthands $\phi_{ij} = -i\epsilon \sum_\tau \overline{c}_{i\tau} d_{j\tau}$ and $\phi_{ij}^* = -i\epsilon \sum_\tau \overline{d}_{j\tau} c_{i\tau}$. In order to obtain the Gaussian average of this quantity over the distribution $\{V_{ij}\}$ we need the following intermediate result (see Appendix A.3.6 for a proof):

$$
\overline{V_a^* V_b e^{\sum_m V_m \phi_m + V_m^* \phi_m^*}} = \begin{cases} (V^2 + V^4 \phi_a \phi_a^*) e^{\sum \phi \phi^*} & a = b \\ V^4 \phi_a \phi_b^* e^{\sum \phi \phi^*} & a \neq b \end{cases} \tag{A.13}
$$

this then allows us to write

$$
\overline{V_{ij}^* V_{kl} e^{\sum_{ij} \phi_{ij} V_{ij} + \phi_{ij}^* V_{ij}^*}} = \delta_{ik}\delta_{jl} \left[V^2 + V^4 \phi_{ij} \phi_{ij}^* \right] + (1 - \delta_{ik}\delta_{jl}) V^4 \phi_{ij} \phi_{kl}^*
$$

In large N, M limit, only the V^2 term survives to leading order inside the path integral. Only second and third terms include terms of order V^2 and we only keep these terms in the large N, M limit. We then end up with

$$
\begin{aligned}
C_{II}(\tau_1, \tau_2) = -ie^2 \int \mathcal{D}[c,d] e^{iS_c + iS_d} \sum_{ij} V^2 [&\overline{d}_{j\tau_1} c_{i\tau_1} \overline{c}_{i\tau_2} d_{j\tau_2} \\
&+ \overline{c}_{i\tau_1} d_{j\tau_1} \overline{d}_{j\tau_2} c_{i\tau_2}] e^{\sum \phi \phi^*}
\end{aligned}
$$

Rearranging this expression yields

$$
\begin{aligned}
C_{II}(\tau_1, \tau_2) = iV^2 e^2 NM \int \mathcal{D}[c,d] e^{iS_c + iS_d + \sum \phi \phi^*} &\underbrace{\left(\frac{1}{N} \sum_i c_{i\tau_1} \overline{c}_{i\tau_2} \right)}_{iG(\tau_1, \tau_2)} \\
\times \underbrace{\left(\frac{1}{M} \sum_j d_{j\tau_2} \overline{d}_{j\tau_1} \right)}_{i\mathcal{G}(\tau_2, \tau_1)} &+ \underbrace{\left(\frac{1}{N} \sum_i c_{i\tau_2} \overline{c}_{i\tau_1} \right)}_{iG(\tau_2, \tau_1)} \underbrace{\left(\frac{1}{M} \sum_j d_{j\tau_1} \overline{d}_{j\tau_2} \right)}_{i\mathcal{G}(\tau_1, \tau_2)}
\end{aligned} \tag{A.14}
$$

where the expressions in brackets above yield the Green's functions G and $\mathcal{G}$ in large-N saddle point after disorder averaging and Hubbard-Stratanovich

decoupling. Recall we had suppressed the denominator in $V_{ij} = V_{ij}/(NM)^{1/4}$ Therefore we should also have $V^2 \to V^2/\sqrt{NM}$. We then obtain the expression:

$$C_{II}(\tau_1, \tau_2) = -ie^2V^2\sqrt{NM}\left[G(\tau_1, \tau_2)\mathcal{G}(\tau_2, \tau_1) + \mathcal{G}(\tau_1, \tau_2)G(\tau_2, \tau_1)\right]$$

Here τ_1, τ_2 are defined on the Keldysh contour. We can analytically continue this expression to obtain $\mathrm{Im}C^R_{II}(t_1, t_2)$.

A.3 Current at Saddle Point

In the following, we derive a formula for the current between two islands using the Keldysh formalism. Our approach is similar to the work of Meir and Wingreen [19]. We start with a current operator and then evaluate its expectation value while considering coupling between the two sites to all orders. The formula we derive applies when the couplins between the two sites are Gaussian random of the form (2.21) and is valid as long as the individual Hamiltonians at each island admit "classical" large-N saddle point solutions. For instance, the formula is valid even if both islands are SYK_4 like. The current operator (rate of change of the charge on the lead) is given by

$$I = -ie\sum_{ab} V_{ab}c^\dagger_a\psi_b - V^*_{ab}\psi^\dagger_b c_a$$

Note that we suppress the denominator in $V_{ij} = V_{ij}/(NM)^{1/4}$ To evaluate the expectation value of the current, we need an expression for the time (contour) ordered operator under disorder average:

$$\overline{V_{ab}\langle\hat{T}c^\dagger_a(\tau_1)\psi_b(\tau_2)\rangle}$$

and similarly $\overline{V^*_{ab}\langle\hat{T}\psi^\dagger_b(\tau_1)c_a(\tau_2)\rangle}$ which appears due to the second term in the current expression we have above. The above correlator (before disorder average) can be written in the path integral formalism as following:

$$\sum_{ab} V_{ab}\left(i\langle\hat{T}c^\dagger_a(\tau_1)\psi_b(\tau_2)\rangle\right) = i\sum_{ab} V_{ab}\frac{\int_{\mathcal{C}}\mathcal{D}[c,\psi]\overline{c_a}(\tau_1)\psi_b(\tau_2)\exp(iS)}{\int_{\mathcal{C}}\mathcal{D}[c,\psi]\exp(iS)}$$

where the Keldysh action S is given by

$$S = S_c + S_\psi - \int d\tau H_{c\psi}(\tau)$$

Here we split the action for c and ψ fermions from the term in the Hamiltonian that couples the two flavours which we label by $H_{c\psi}$. Keldysh formalism is especially convenient for performing disorder averages since the denominator $Z = \mathcal{D}[c,\psi]\exp(iS)$ for the above correlator expression is generically unity. [16] **Therefore, for the following discussion we can ignore the denominator and proceed with the averaging.** We consider the coupling term to be of the form

$$H_{c\psi} = \sum_{ij} V_{ij} c_i^\dagger \psi_j + V_{ij}^* \psi_j^\dagger c_i$$

to simplify the notation, we write the time (contour) integrals as sums $\int \to \epsilon \sum_\tau$ and change the time index notation on fermionic Grassman numbers as the following: $c_a(\tau) \to c_{a\tau}$. Now we can rewrite the expression (A.3) as:

$$\overline{\sum_{ab} V_{ab} i\langle \hat{T} c_a^\dagger(\tau_1)\psi_b(\tau_2)\rangle} = i\sum_{ab}\int_{\mathcal{C}} \mathcal{D}[c,\psi]\bar{c}_{a\tau_1}\psi_{b\tau_2} e^{iS_c+iS_\psi} \times \overline{V_{ab}\exp\left(-i\epsilon\sum_{ij\tau} V_{ij}\bar{c}_{i\tau}\psi_{j\tau}\right)\exp\left(-i\epsilon\sum_{ij\tau} V_{ij}^*\overline{\psi}_{j\tau}c_{i\tau}\right)} \quad \text{(A.15)}$$

Now we would like to compute the average of this quantity over complex Gaussian distributions V_{ij} with variance V^2. Here we assume that among all i,j labels, V_{ij} distributions are independent. We are interested in the identity:

$$\overline{V_{ab} e^{\left(\sum_{ij} V_{ij}\phi_{ij} + \sum_{ij} V_{ij}^*\phi_{ij}^*\right)}} = V^2\phi_{ab}^* \times \overline{e^{\left(\sum_{ij} V_{ij}\phi_{ij} + \sum_{ij} V_{ij}^*\phi_{ij}^*\right)}} \quad \text{(A.16)}$$

where we defined the shorthands $\phi_{ij} = -i\epsilon\sum_\tau \bar{c}_{i\tau}\psi_{j\tau}$ and $\phi_{ij}^* = -i\epsilon\sum_\tau \overline{\psi}_{j\tau}c_{i\tau}$. Note that star (*) here does not mean complex conjugate. Proof of this identity is given in appendix A.3.5. The average on the RHS above can be evaluated by completing Gaussian integrals to square (see appendix A.3.4) Replacing ϕ_{ij}s back, we obtain (the expression under the bar in equation (A.15)):

$$-iV^2\int d\tau''\overline{\psi}_{b\tau''}c_{a\tau''}\exp\left(V^2\int d\tau d\tau'\left(\sum_i \bar{c}_{i\tau}c_{i\tau'}\right)\left(\sum_j \overline{\psi}_{j\tau'}\psi_{j\tau}\right)\right)$$

where we replaced sums with integrals over time contours back $\epsilon \sum_\tau \to \int$: finally we plug this expression into (A.15):

$$\overline{V_{ab} i\langle \hat{T} c_a^\dagger(\tau_1)\psi_b(\tau_2)\rangle} = -V^2 \int_{\mathcal{C}} d\tau'' \int \mathcal{D}[c,\psi] \sum_a \overline{c}_{a\tau_1} c_{a\tau''} \sum_b \overline{\psi}_{b\tau''}\psi_{b\tau_2} \\ \times e^{iS_c + iS_\psi} e^{V^2 \int d\tau d\tau' \left(\sum_i \overline{c}_{i\tau} c_{i\tau'}\right)\left(\sum_j \overline{\psi}_{j\tau'}\psi_{j\tau}\right)}$$

Now let us decouple the exponential by introducing a bosonic unity:

$$\int \mathcal{D}[P,Q] \exp\left(-\int d\tau d\tau' P_{\tau\tau'} Q_{\tau'\tau}\right) = 1 \tag{A.17}$$

the exponential in the path integral above can we written as:

$$e^{V^2 \int d\tau d\tau' \ldots} = \int \mathcal{D}[P,Q] e^{\int d\tau d\tau' \left[V^2 \sum_i \overline{c}_{i\tau} c_{i\tau'} \sum_j \overline{\psi}_{j\tau'}\psi_{j\tau} - P_{\tau\tau'} Q_{\tau'\tau}\right]}$$

now we do the following change of variables $P_{\tau\tau'} \to P_{\tau\tau'} + V \sum_i \overline{c}_{i\tau} c_{i\tau'}$ and $Q_{\tau'\tau} \to Q_{\tau'\tau} + V \sum_j \overline{\psi}_{j\tau'}\psi_{j\tau}$ cancelling the quadratic fermion cross term:

$$e^{V^2 \int d\tau d\tau' \ldots} = \int \mathcal{D}[P,Q] e^{\int d\tau d\tau' \left[-P_{\tau\tau'} Q_{\tau'\tau} + V P_{\tau\tau'} \sum_j \overline{\psi}_{j\tau'}\psi_{j\tau} + V Q_{\tau'\tau} \sum_i \overline{c}_{i\tau} c_{i\tau'}\right]}$$

But this completely decouples two different flavours of fermions, allowing us to rewrite the combined path integral as a product:

$$\overline{V_{ab}\langle i\hat{T} c_a^\dagger(\tau_1)\psi_b(\tau_2)\rangle} = -V^2 \int_{\mathcal{C}} d\tau'' \int \mathcal{D}[P,Q] e^{-\int_{\tau\tau'} P_{\tau\tau'} Q_{\tau'\tau}} \\ \times \int \mathcal{D}[c] \sum_a \overline{c}_{a\tau_1} c_{a\tau''} e^{iS_c} e^{V\left(\int_{\tau\tau'} Q_{\tau'\tau} \sum_i \overline{c}_{i\tau} c_{i\tau'}\right)} \\ \times \int \mathcal{D}[\psi] \sum_b \overline{\psi}_{b\tau''}\psi_{b\tau_2} e^{iS_d} e^{V\left(\int_{\tau\tau'} P_{\tau\tau'} \sum_j \overline{\psi}_{j\tau'}\psi_{j\tau}\right)} \tag{A.18}$$

A.3.1 Evaluation of Gaussian integrals

We would like to evaluate the expression (A.18) above. If fermionic degrees of freedom are already noninteracting (bilinear), their respective actions can be Gaussian integrated. Let us consider the following part of the above action:

$$\int \mathcal{D}[c] \sum_a \overline{c}_{a\tau_1} c_{a\tau''} e^{iS_c} e^{V\left(\int_{\tau\tau'} Q_{\tau'\tau} \sum_i \overline{c}_{i\tau} c_{i\tau'}\right)} \\ = \frac{1}{V} \frac{\delta}{\delta Q_{\tau''\tau_1}} \int \mathcal{D}[c] e^{iS_c} e^{V\left(\int_{\tau\tau'} Q_{\tau'\tau} \sum_i \overline{c}_{i\tau} c_{i\tau'}\right)} \tag{A.19}$$

In RHS above, we simplified the expression by writing it with a functional derivative. Note that the path integral on the RHS must be a Gaussian integral or it can be brought to a Gaussian form by further decoupling with HS transformations. This will introduce more bosonic fields which appear as terms like $Q_{\tau'\tau}$ in the exponential as well as overall bosonic path integrals for the correlator expression. Let us assume without loss of generality that $S_c = \int_\tau \sum_i \bar{c}_{i\tau}[G_0^{-1}\delta_{\tau\tau'} + B_{\tau\tau'}]c_{i\tau'}$ has a Gaussian form where $B_{\tau\tau'}$ represent the possible the extra terms we just mentioned above. In the presence of such fields, overall path integrals $\int \mathcal{D}B$ over these degrees of freedom are implied. ($G_0^{-1} = i\partial\tau$) The Gaussian integral above then can be written as:

$$\begin{aligned}
&\int \mathcal{D}[c] \exp\left(\int_{\tau\tau'} \sum_i \bar{c}_{i\tau}\left[iG_0^{-1}\delta_{\tau\tau'} + B_{\tau\tau'} + VQ_{\tau'\tau}\right] c_{i\tau'}\right) \\
&= \prod_i \int \mathcal{D}[c_i] \exp\left(-\sum_{\tau\tau'} \bar{c}_{i\tau} \underbrace{(-\epsilon^2)\left[iG_0^{-1}\delta_{\tau\tau'} + B_{\tau\tau'} + VQ_{\tau'\tau}\right]}_{C_i(\tau,\tau')} c_{i\tau'}\right) \\
&= \prod_i \det(C_i) = \exp(\sum_i \mathrm{Tr}[\log(C_i)]) = \exp(N\mathrm{Tr}[\log(C)])
\end{aligned} \tag{A.20}$$

The last equality holds since $C_i = C$ is the same for all i in the sum. Notice that $C(\tau,\tau') = -i\epsilon^2 G^{-1}(\tau,\tau')$ where G is the Green's function renormalized due to V couplings (as well as extra B fields). We read off this relation from the above form of the Gaussian integral. If we go back to the above expression (A.19) to evaluate the path integral,

$$\begin{aligned}
&\int \mathcal{D}[c] \sum_a \bar{c}_{a\tau_1} c_{a\tau''} e^{iS_c} e^{V\left(\int_{\tau\tau'} Q_{\tau'\tau} \sum_i \bar{c}_{i\tau} c_{i\tau'}\right)} = \frac{1}{V}\frac{\delta}{\delta Q_{\tau''\tau_1}} e^{N\mathrm{Tr}[\log(C)]} \\
&= N e^{N\mathrm{Tr}\log(C)}(-\epsilon^2) C(\tau'',\tau_1)^{-1} = -iNG(\tau'',\tau_1) e^{N\mathrm{Tr}[\log(C)]}
\end{aligned} \tag{A.21}$$

where in the last step we used the relation between C and G that we found above. **Note that the above expression did not depend on the presence or form of additional B bosonic degrees of freedom. They will vanish under the functional derivative with respect to Q.** The expression for the the other path integral similarly follows. To summarize these results, we have:

$$\int \mathcal{D}[c] \sum_a \bar{c}_{a\tau_1} c_{a\tau''} e^{iS_c} e^{V\left(\int_{\tau\tau'} Q_{\tau'\tau} \sum_i \bar{c}_{i\tau} c_{i\tau'}\right)} = -iNG(\tau'',\tau_1) e^{N\mathrm{Tr}[\log(C)]} \tag{A.22}$$

$$\int \mathcal{D}[\psi] \sum_b \overline{\psi}_{b\tau''} d\psi_{b\tau_2} e^{iS_\psi} e^{V(\int_{\tau\tau'} P_{\tau\tau'} \sum_j \overline{\psi}_{j\tau'} d_{j\tau})} = -iM\mathcal{G}(\tau_2, \tau'') e^{M\mathrm{Tr}[\log(D)]} \tag{A.23}$$

where

$$C_{\alpha\beta} = (-\epsilon^2) \left[iG_0^{-1}\delta_{\alpha\beta} + B_{\alpha\beta} + VQ_{\beta\alpha} \right] = -i\epsilon^2 G^{-1}_{\alpha\beta} \tag{A.24}$$

$$D_{\alpha\beta} = (-\epsilon^2) \left[i\mathcal{G}_0^{-1}\delta_{\alpha\beta} + B'_{\alpha\beta} + VP_{\beta\alpha} \right] = -i\epsilon^2 \mathcal{G}^{-1}_{\alpha\beta} \tag{A.25}$$

The expression for the ψ fermions is very similar - note that we introduced B' similar to the B we had for c fermions. Now we use equations (A.22) and (A.23) in the original path integral (A.18).

$$\begin{aligned} &\overline{\sum_{ab} V_{ab} i\langle \hat{T} c_a^\dagger(\tau_1) d_b(\tau_2)\rangle} \\ &\qquad = MNV^2 \int_{\mathcal{C}} d\tau'' \int \mathcal{D}[P, Q, B, B'] \mathcal{G}(\tau_2, \tau'') G(\tau'', \tau_1) \\ &\qquad\qquad \times e^{-\int B, B' \ldots} e^{-\int_{\tau\tau'} P_{\tau\tau'} Q_{\tau'\tau} + N\mathrm{Tr}[\log(C)] + M\mathrm{Tr}[\log(D)]} \end{aligned} \tag{A.26}$$

A.3.2 Effective action and the large-N limit

To compute the effective action at saddle point we would have followed the exact same steps to obtain the disorder averaged expression for $Z = 1$ except that we would not take the functional derivatives to bring down the Green's functions in the fermionic path integrals as we did in (A.21)

$$Z = \int \mathcal{D}[P, Q, B, B'] e^{-\int B, B' \ldots} e^{-\int_{\tau\tau'} P_{\tau\tau'} Q_{\tau'\tau} + N\mathrm{Tr}[\log(C)] + M\mathrm{Tr}[\log(D)]} \tag{A.27}$$

we represent the additional bosonic fields by B and B' which appear after decoupling of interacting fermionic degrees of freedom. The expression $e^{-\int B, B' \ldots}$ is a shorthand for these additional terms in the action. We can rewrite the above expression as

$$Z = \int \mathcal{D}[P, Q, B, B'] e^{-S_{eff}[P, Q, B, B']}$$

where

$$\begin{aligned} S_{eff}[P, Q, B, B'] &= \int B, B' \ldots \\ &\quad + \int_{\tau\tau'} P_{\tau\tau'} Q_{\tau'\tau} - N\mathrm{Tr}[\log C(B, Q)] - M\mathrm{Tr}[\log D(B', Q)] \end{aligned} \tag{A.28}$$

we can obtain the saddle point equations with:

$$\frac{\delta S_{eff}}{\delta P_{ab}} = 0 \qquad \frac{\delta S_{eff}}{\delta Q_{ab}} = 0 \qquad \frac{\delta S_{eff}}{\delta B} = 0 \quad ...$$

For a general formula, however, we do not need to obtain these equations explicitly. Fermionic degrees of freedom are integrated out but they depend on the bosonic fields. Next step is to evaluate the bosonic path integrals. We can approximate these path integrals with the saddle point approximation. The crucial observation is that as long as the fluctuations with respect to the saddle point vanish in the large-N limit, the path integral will be given by the classical action S^0_{eff} evaluated at the saddle point. In large-N limit, saddle point approximation then reads:

$$Z = \int \mathcal{D}[P, Q, B, B'] e^{-S_{eff}[P,Q,B,B']} \approx e^{-S_{eff}[P^0,Q^0,B^0,B'^0]} = 1$$

since in Keldysh formalism $Z = 1$. Therefore we obtain:

$$e^{-S_{eff}[P^0,Q^0,B^0,B'^0]} = 1$$

where the superscript means the saddle point values of the bosonic fields. Now we go back to the numerator we obtained above (equation (A.26)). Note that we can do the saddle point approximation that we used for Z as it is essentially the same expression except that it also contains the Green's functions before the exponent. Note that the Green's functions $G(B, Q)$ and $\mathcal{G}(B', P)$ depend on the fields $P, Q, B, B'...$ (eqns A.24, A.25) and they can not be taken outside the integral immediately. But in the large-N limit, their fluctuations with respect to the saddle point vanish and we can replace them with their values at the saddle point and we can take them outside the path integral. Therefore, in large-N limit, we can rewrite the numerator (A.26) as:

$$\overline{\sum_{ab} V_{ab} i\langle \hat{T} c^\dagger_a(\tau_1)\psi_b(\tau_2)\rangle} = MNV^2 \int_{\mathcal{C}} d\tau'' \underbrace{\mathcal{G}(\tau_2, \tau'')G(\tau'', \tau_1)}_{\text{saddle-point values}}$$
$$\times \underbrace{\int \mathcal{D}[P, Q, B, B'] e^{-\int B,B'...} e^{-\int_{\tau\tau'} P_{\tau\tau'}Q_{\tau'\tau} + N\mathrm{Tr}[\log(C)] + M\mathrm{Tr}[\log(D)]}}_{e^{-S_{eff}[P^0,Q^0,B^0,B'^0]}=1} \quad \text{(A.29)}$$

but note that the rest of the integral is nothing but $Z = e^{-S_{eff}[P^0,Q^0,B^0,B'^0]} = 1$. Therefore, we arrive at the disorder averaged saddle-point current formula:

$$\overline{\sum_{ab} V_{ab} i\langle \hat{T} c^\dagger_a(\tau_1)\psi_b(\tau_2)\rangle} = MNV^2 \int_{\mathcal{C}} d\tau'' \mathcal{G}(\tau_2, \tau'')G(\tau'', \tau_1) \qquad \text{(A.30)}$$

$$\overline{\sum_{ab} V_{ab}^* i\langle \hat{T}\psi_b^\dagger(\tau_1)c_a(\tau_2)\rangle} = MNV^2 \int_{\mathcal{C}} d\tau'' G(\tau_2,\tau'')\mathcal{G}(\tau'',\tau_1) \tag{A.31}$$

where G and $\mathcal{G}$ are the saddle point Green's functions evaluated in the presence of all interactions.

A.3.3 Analytic continuation

We are interested in the real-time quantitites:

$$C_1^<(t_1,t_2) = \overline{\sum_{ab} V_{ab} i\langle c_a^\dagger(t_2)\psi_b(t_1)\rangle} \qquad C_2^<(t_1,t_2) = \overline{\sum_{ab} V_{ab}^* i\langle \psi_b^\dagger(t_2)c_a(t_1)\rangle}$$

with these we can write the current expectation value as:

$$\langle I\rangle = \lim_{t_1,t_2\to t} -e\left(C_1^<(t_1,t_2) - C_2^<(t_1,t_2)\right)$$

We can obtain these lesser Green's functions by using Langareth's rules [20]. The expression

$$C(\tau_1,\tau_2) = \int_{\mathcal{C}} d\tau' A(\tau_1,\tau')B(\tau',\tau_2)$$

on time ordered contour can be analytically continued to:

$$C^<(t_1,t_2) = \int_{-\infty}^{\infty} dt' A^r(t_1,t')B^<(t',t_2) + A^<(t_1,t')B^a(t',t_2)$$

using this expression for equations (A.30) and (A.31) The current expression then becomes:

$$\begin{aligned}\langle I\rangle = -eNMV^2 \int dt' &\mathcal{G}^r(t,t')G^<(t',t) + \mathcal{G}^<(t,t')G^a(t',t) \\ &- G^r(t,t')\mathcal{G}^<(t',t) - G^<(t,t')\mathcal{G}^a(t',t)\end{aligned}$$

Fourier transforming (assume time translational invariance), we arrive at the final formula:

$$\langle I\rangle = -eNMV^2 \int d\omega \left\{G^<(\omega)\left[\mathcal{G}^r(\omega) - \mathcal{G}^a(\omega)\right] - \mathcal{G}^<(\omega)\left[G^r(\omega) - G^a(\omega)\right]\right\} \tag{A.32}$$

we can simplify this further by using the relation: $G^R - G^A = 2i\text{Im}G^R = -iA(\omega)$

$$\langle I \rangle = ieNMV^2 \int d\omega \left\{ G^<(\omega)\mathcal{A}(\omega) - \mathcal{G}^<(\omega)A(\omega) \right\} \tag{A.33}$$

Recall we had suppressed the denominator in $V_{ij} = V_{ij}/(NM)^{1/4}$ Therefore we should also have $V^2 \to V^2/\sqrt{NM}$.

$$\boxed{\langle I \rangle = ie\sqrt{NM}V^2 \int d\omega \left\{ G^<(\omega)\mathcal{A}(\omega) - \mathcal{G}^<(\omega)A(\omega) \right\}} \tag{A.34}$$

A.3.4 Disorder averaging of the coupling

We would like to evaluate

$$\overline{\exp\left(\sum_{ij} V_{ij}\phi_{ij} + \sum_{ij} V_{ij}^*\phi_{ij}^* \right)}$$

let us suppress the indices $ij \to i$ for simplicity. We can rewrite this expression as:

$$\overline{\exp\left(\sum_{i} V_i\phi_i + V_i^*\phi_i^* \right)} = \prod_i \overline{\exp\left(V_i\phi_i + V_i^*\phi_i^*\right)}$$

since all V_i are independent random variables, it suffices that we evaluate the average (for $\Gamma = V^2$ where V is the variance

$$\overline{\exp\left(V_i\phi_i + V_i^*\phi_i^*\right)} = \int dz \frac{e^{-zz^*/\Gamma}}{\pi\Gamma} e^{(z\phi + z^*\phi^*)}$$

If we switch to real variables $z = x + iy$:

$$\overline{\exp\left(V_i\phi_i + V_i^*\phi_i^*\right)} = \int \frac{dxdy}{\pi\Gamma} \exp(-\frac{x^2+y^2}{\Gamma}) + (x+iy)\phi + (x-iy)\phi^*$$

if we split the x and y integrals and complete them to square, we are left with:

$$= \underbrace{\frac{1}{\pi\Gamma} \int dxdy e^{-(x^2+y^2)/\Gamma}}_{=1} e^{\Gamma\phi\phi^*}$$

for the last step we assumed that ϕ and ϕ^* commute. This is true in our case since they are Grassman bilinears. Therefore, we find that:

$$\overline{\exp\left(\sum_{ij} V_{ij}\phi_{ij} + V_{ij}^*\phi_{ij}^* \right)} = \exp\left(V^2 \sum_{ij} \phi_{ij}\phi_{ij}^* \right)$$

A.3.5 Proof of the Gaussian average identity (A.16)

We define the complex Gaussian distribution as:

$$p(z) = \frac{e^{-zz^*/\Gamma}}{\pi\Gamma}$$

Now let us further suppress the pair labels $i, j \to i$ and $a, b \to a$ without loss of generality. Then if we evaluate the variance σ we find $\langle zz^* \rangle = \Gamma = \sigma^2$. Now we split the sums in the exponential as following:

$$\begin{aligned}\overline{V_a e^{V_a\phi_a} e^{V_a^*\phi_a^*} \exp\left(\sum_{i\neq a} V_i\phi_i\right) \exp\left(\sum_{i\neq a} V_i^*\phi_i^*\right)} \\ = \overline{V_a e^{V_a\phi_a} e^{V_a^*\phi_a^*}} \times \overline{\exp\left(\sum_{i\neq a} V_i\phi_i\right) \exp\left(\sum_{i\neq a} V_i^*\phi_i^*\right)}\end{aligned} \tag{A.35}$$

since the distribution V_a is independent of V_i for all $i \neq a$, we can factor the averages as above. Now we focus on the first factor and the average over V_a as we expand the exponentials:

$$\overline{V_a e^{V_a\phi_a} e^{V_a^*\phi_a^*}} = \overline{\sum_{mn} V_a \frac{(V_a^*\phi_a^*)^n}{n!} \frac{(V_a\phi_a)^m}{m!}} = \sum_{mn} \overline{V_a (V_a^*)^m (V_a)^n} \frac{(\phi_a^*)^m}{m!} \frac{(\phi_a)^n}{n!} \tag{A.36}$$

Now we use a version of Wick's theorem for complex Gaussian integrals. This theorem tells us that the average of a product of Gaussian distributed variables can we factored into averages of all pairings. For example:

$$\langle z_i^* z_j z_k^* z_l \rangle = \langle z_i^* z_j \rangle \langle z_k^* z_l \rangle + \langle z_i^* z_l \rangle \langle z_k^* z_j \rangle$$

Only pairings of type $\langle z^* z \rangle = \sigma^2$ survive. It can be shown that $\langle zz \rangle = \langle z^* z^* \rangle = 0$. Therefore we have

$$\boxed{\langle V_{ij} V_{kl}^* \rangle = V^2 \delta_{ik} \delta_{jl}}$$

Now go back to the average we wish to evaluate:

$$\overline{V_a (V_a^*)^m (V_a)^n}$$

According to Wick's theorem, we can factor this product into all possible pairings of Vs and V^*s. Let us focus on the first V_a that occurs in the

product. For this expression to survive the average, this first V_a must be paired with a V_a^*. There are m different ways of doing this and they are all identical:

$$\begin{aligned}\overline{V_a(V_a^*)^m(V_a)^n} &= m \times \overline{V_a V_a^*} \times \left(\text{all pairings of } (V_a^*)^{m-1}(V_a)^n\right) \\ &= m \times \underbrace{\overline{V_a V_a^*}}_{V^2} \times \overline{(V_a^*)^{m-1}(V_a)^n}\end{aligned}$$

if we use this result in above expression (A.36), we obtain

$$\begin{aligned}\overline{V_a e^{V_a\phi_a} e^{V_a^*\phi_a^*}} &= V^2\phi_a^* \sum_{mn} \overline{(V_a^*)^{m-1}(V_a)^n} \frac{(\phi_a^*)^{m-1}}{(m-1)!}\frac{(\phi_a)^n}{n!} \\ &= V^2\phi_a^* \overline{\sum_{mn} \frac{(V_a^*\phi_a^*)^{m-1}}{(m-1)!}\frac{(V_a\phi_a)^n}{n!}}\end{aligned}$$

but now we see the averaged expression in the above line is nothing but the product of exponentials. Plugging this result back into (A.35)

$$\overline{V_a \exp\left(\sum_i V_i\phi_i\right)\exp\left(\sum_i V_i^*\phi_i^*\right)} = V^2\phi_a^* \overline{e^{V_a\phi_a}e^{V_a^*\phi_a^*}} \times \overline{e^{\sum_{i\neq a} V_i\phi_i} e^{\sum_{i\neq a} V_i^*\phi_i^*}} \tag{A.37}$$

but again, the product of these two averages can be combined because averages of V_i are independent. Then we finish the proof state our intermediate result about V averages here:

$$\boxed{\overline{V_{ab}\exp\left(\sum_{ij} V_{ij}\phi_{ij} + \sum_{ij} V_{ij}^*\phi_{ij}^*\right)} = V^2\phi_{ab}^* \times \overline{\exp\left(\sum_{ij} V_{ij}\phi_{ij} + \sum_{ij} V_{ij}^*\phi_{ij}^*\right)}} \tag{A.38}$$

A.3.6 Proof of Gaussian Identity (A.13)

In this section, we prove the following identity:

$$\overline{V_a^* V_b e^{\sum_m V_m\phi_m + V_m^*\phi_m^*}} = \begin{cases} (V^2 + V^4\phi_a\phi_a^*)e^{\sum\phi\phi^*} & a = b \\ V^4\phi_a\phi_b^* e^{\sum\phi\phi^*} & a \neq b \end{cases}$$

Case 1, $a = b$

The above expression reduces to:

$$\overline{V_a^* V_b \exp\left(\sum_m V_m\phi_m + V_m^*\phi_m^*\right)} = \overline{V_a^* V_a \exp\left(V_a\phi_a + V_a^*\phi_a^*\right)} \times \overline{\exp\left(\sum_{m\neq a} V_m\phi_m + V_m^*\phi_m^*\right)} \quad \text{(A.39)}$$

The first factor $\overline{V_a^* V_a \exp\left(V_a\phi_a + V_a^*\phi_a^*\right)}$ can be written as

$$\overline{\sum_{m,n} V_a^* V_a \frac{V_a^m \phi_a^m}{m!}\frac{(V_a^*)^n(\phi_a^*)^n}{n!}} = \overline{V_a^* V_a}\overline{\sum_{m,n}\frac{V_a^m\phi_a^m}{m!}\frac{(V_a^*)^n(\phi_a^*)^n}{n!}} + \sum_{m,n}\frac{m\times\overline{V_a^*V_a}}{m!}\frac{n\times\overline{V_aV_a^*}}{n!}\overline{V_a^{m-1}(V_a^*)^{n-1}}\phi_a^m(\phi_a^*)^n$$

where used a variant of the Wick's theorem we introduced in the previous section. While the first term on the RHS is the pairing of V_a and V_a^* that was outside the exponential initially, the second term involves the pairings of these two factors with the exponential series. These two terms can again be written up as exponentials:

$$= (V^2 + V^4\phi_a\phi_a^*)\overline{\exp\left(V_a\phi_a + V_a^*\phi_a^*\right)}$$

completing the proof, where we used $\langle V_a V_b^*\rangle = V^2\delta_{ab}$.

Case 2, $a \neq b$

In this case we can split the averages as following:

$$\overline{V_a^* V_b \exp\left(\sum_m V_m\phi_m + V_m^*\phi_m^*\right)} = \overline{V_a^*\exp\left(V_a\phi_a + V_a^*\phi_a^*\right)} \times \overline{V_b\exp\left(V_a\phi_a + V_a^*\phi_a^*\right)} \times \overline{e^{\left(\sum_{m\neq a,b} V_m\phi_m + V_m^*\phi_m^*\right)}}$$

we can use the result (A.37) from the previous section to simplify this expression

$$= V^2\phi_a\overline{\exp\left(V_a\phi_a + V_a^*\phi_a^*\right)} \times V^2\phi_b^*\overline{\exp\left(V_b\phi_b + V_b^*\phi_b^*\right)} \times \overline{e^{\left(\sum_{m\neq a,b} V_m\phi_m + V_m^*\phi_m^*\right)}}$$
$$= V^4\phi_a\phi_b^*\overline{e^{\left(\sum_m V_m\phi_m + V_m^*\phi_m^*\right)}}$$

completing the proof.